

ORIGINAL PAPER

A. J. L. Harris · L. P. Flynn · L. Keszthelyi
 P. J. Mouginiis-Mark · S. K. Rowland · J. A. Resing

Calculation of lava effusion rates from Landsat TM data

Received: 25 July 1997 / Accepted: 26 February 1998

Abstract We present a thermal model to calculate the total thermal flux for lava flowing in tubes, on the surface, or under shallow water. Once defined, we use the total thermal flux to estimate effusion rates for active flows at Kilauea, Hawaii, on two dates. Input parameters were derived from Landsat Thematic Mapper (TM), field and laboratory measurements. Using these parameters we obtain effusion rates of 1.76 ± 0.57 and $0.78 \pm 0.27 \text{ m}^3 \text{ s}^{-1}$ on 23 July and 11 October 1991, respectively. These rates are corroborated by field measurements of 1.36 ± 0.14 and $0.89 \pm 0.09 \text{ m}^3 \text{ s}^{-1}$ for the same dates (Kauahikaua et al. 1996). Using weather satellite (AVHRR) data of lower spatial resolution, we obtain similar effusion rates for an additional 26 dates between the two TM-derived measurements. We assume that, although total effusion rates at the source declined over the period, the shut down of the ocean entry meant that effusion rates for the surface flows alone remained stable. Such synergetic use of remotely sensed data provides measurements that can (a) contribute to monitoring flow-field evolution, and (b) provide reliable numerical data for input into rheological and thermal models. We look forward to being able to produce estimates for effusion rates using data from high-spatial-resolution sensors in the earth observing system (EOS) era, such as Landsat 7, the hyperspectral

imager, the advanced spaceborne thermal emission spectrometer, and the advanced land imager.

Key words TM · Lava flow · Thermal flux · Effusion rates · AVHRR · Pu'u 'O'o–Kupaianaha

Introduction

Since the mid-1980s many studies have shown how space-based thermal observations can contribute to the monitoring and analysis of an active lava flow field. Numerous parameters have been measured, including flow length, width and area, crust temperature and thickness, core temperature, skylight area, thermal flux, and effusion rates (Pieri et al. 1990; Oppenheimer 1991; Flynn et al. 1994; Harris et al. 1997a, b). The 30-m spatial resolution of the Landsat Thematic Mapper (TM) has proven to be very useful for spatially detailed analysis of active lava bodies (e.g., Rothery et al. 1988; Pieri et al. 1990; Oppenheimer 1991; Oppenheimer et al. 1993; Bhattacharya et al. 1993; Gupta and Badarinath 1993; Flynn et al. 1994; Andres and Rose 1995). However, TM data are available only once every 16 days, and many aspects of an ongoing eruption will change during the time period between acquisitions. Such changes may be identified using low spatial resolution ($\sim 1 \text{ km}$) data provided by weather satellites at a much higher temporal frequency, once every 6 h in the case of the advanced very high resolution radiometer (e.g., Harris et al. 1995, 1997a, b).

For analysis of active flows, heat flux is an important parameter to measure. Flynn et al. (1994) used TM data of Kilauea (Hawaii) to map and investigate radiant heat-flux density and to establish a chronology of flow emplacement. The purpose of this paper is to improve on this first investigation by modeling the thermal flux from active lava flows, determining the total thermal flux for all active flows apparent on the TM scene, and converting total thermal flux to an instantaneous eruption rate or effusion rate.

Editorial responsibility: M.R. Carroll

Andrew J. L. Harris (✉)¹ · Luke P. Flynn · Laszlo Keszthelyi
 Peter J. Mouginiis-Mark · Scott K. Rowland
 Hawaii Institute for Geophysics and Planetology, SOEST,
 2525 Correa Road, Honolulu, HI 96822, USA

Joseph A. Resing²
 Department of Oceanography, SOEST, 2525 Correa Road,
 Honolulu, HI 96822, USA

Present addresses:

¹Department of Earth Sciences, The Open University,
 Milton Keynes MK7 6AA, UK

²NOAA-PMEL, Building 3, 7600 Sand Point Way NE, Seattle,
 WA 98115, USA

Determining volumetric effusion rates for lava flows from space is an important but challenging task. Effusion rates are a major consideration in evaluating flow dynamics and the potential threat posed by a lava flow. Higher effusion rates produce channel-fed flows that are longer, more rapidly moving, voluminous, and areally extensive than flows with low effusion rates (Walker 1973; Wadge 1978; Malin 1980; Pieri and Baloga 1986; Wolfe et al. 1988; Rowland and Walker 1990; Pinkerton and Wilson 1994). Flows with high effusion rate thus have far greater potential to inflict damage on distant communities with less advance warning. For example, the 1983 and 1985 eruptions on Mt. Etna's (Sicily) south flank were of similar duration, lasting 131 and 123 days, respectively. The 1983 eruption was fed by effusion rates of up to 22–44 m³ s⁻¹, and flows extended 7 km to form a 6 km², 100 × 10⁶ m³, flow field (McClelland et al. 1989). In contrast, the 1985 eruption was fed by effusion rates of 0.5–4.5 m³ s⁻¹, which resulted in flows extending 1.8 km to form a 2.2-km², 19 × 10⁶-m³, flow field (McClelland et al. 1989; Harris et al. 1997a). Effusion rate also appears to control the basic flow dynamics. In Hawaii, effusion rates determine the manner in which flows are emplaced. Effusion rates >20 m³ s⁻¹ produce rapidly advancing channelized 'a'a flows, and effusion rates <20 m³ s⁻¹ (but more typically ~5 m³ s⁻¹) produce slowly advancing tube-fed pahoehoe flows (Rowland and Walker 1990).

Measuring effusion rates is therefore of great interest. Field methods for their determination are usually based on estimates of lava channel dimensions and lava flow velocity (e.g., Frazzetta and Romano 1984; Lipman and Banks 1987; McClelland et al. 1989; Barberi et al. 1993). However, errors due to uncertainties in channel dimensions, especially depth, are a major problem (Pinkerton and Sparks 1976; Frazzetta and Romano 1984). Alternatively, if eruption duration is known, accurate post-eruption measurements of total flow-field volume can provide reliable estimates of average effusion rates (e.g., Wadge 1981; Rowland and Munro 1993; Calvari et al. 1994; Reynolds et al. 1995; Rowland 1996). However, these averages will not reveal major variations in effusion rates which have been shown to occur during many basaltic eruptions (Wadge 1981). The very low frequency (VLF) electromagnetic induction method of Kauahikaua et al. (1996) provides a means of estimating cross-sectional areas of the liquid lava within lava tubes. Coupled with velocity measurements made at skylights, VLF allows accurate measurements of instantaneous volumetric flux through the tube. If all the erupted lava passes through the tube, this equals the effusion rate. Techniques capable of measuring effusion rates during an eruption are of particular value since accurate effusion rate estimates are important in hazard prediction, warning, and mitigation.

Herein we extend the thermal approach of Pieri and Baloga (1986) and Harris et al. (1997b) to estimate effusion rates. Firstly, we describe the field setting and

remote sensing data sets that we use to illustrate the utility of the model. Next, we provide three generally applicable thermal models that can be used individually or together to estimate effusion rates for lava flowing in tubes, on the surface, or entering the ocean. We then demonstrate the application of our approach using TM and field data for the Pu'u 'Ō'ō–Kupaianaha eruption at Kilauea (Hawaii) to estimate effusion rates on two dates in 1991 and to monitor the evolution of the flow field. Finally, the temporal context of these observations is provided by a series of advanced very high resolution radiometer (AVHRR) images obtained before, during, and after each of the Landsat observations.

Field setting

The current eruption at Kilauea has now progressed through 55 episodes of activity, with activity beginning at the Pu'u 'Ō'ō vent on 3 January 1983. Until episode 48, episodic eruptions at Pu'u 'Ō'ō exhibited several styles of activity and variable effusion rates. However, episode 48 was characterized by steady lava effusion from a new vent named Kupaianaha at a rate of ~3.5 m³ s⁻¹ that had formed a 75-km² flow field by January 1991 (Wolfe et al. 1988; Heliker and Wright 1991; Mattox et al. 1993). During 1991 lava flux from the Kupaianaha vent declined linearly from 2.9 m³ s⁻¹ in April 1991 to 0.6 m³ s⁻¹ by November 1991, with output ceasing during February 1992 (Kauahikaua et al. 1996). This part of the eruption is ideal for testing remote sensing techniques or models, because the abundant ground-truth data collected by the U.S. Geological Survey's Hawaiian Volcano Observatory (HVO; e.g., Wolfe et al. 1988; Heliker and Wright 1991; Mattox et al. 1993; Mangan et al. 1995; Kauahikaua et al. 1996) provide an excellent means of validation or source of model inputs.

Herein we use both high spatial resolution TM data, higher temporal resolution AVHRR data, and ground-based measurements to show how synergetic use of the data can contribute to measuring, mapping, and monitoring an active lava flow field. We use two cloud-free TM images acquired on 23 July and 11 October 1991 during the waning activity of the Kupaianaha vent. We supplement our coverage with 26 cloud-free AVHRR images acquired between July and October 1991. During this time surface flows issued from a tube system that extended from beneath the frozen surface of the lava lake over the Kupaianaha vent (Fig. 1; GVN 1991b–e). In July and August the main tube, the Wahauala tube, bifurcated at ~180 m elevation to feed a western and an eastern branch. These fed surface flows and lava flows that entered the sea at the Poupou and Paradise Ocean entries, respectively, (Fig. 1a, b; GVN 1991b, c). In September numerous tube-fed surface flows became concentrated on the western side of the flow field, and the Paradise and Poupou entries shut down on 3 and 20 September, respectively (Fig. 1c;

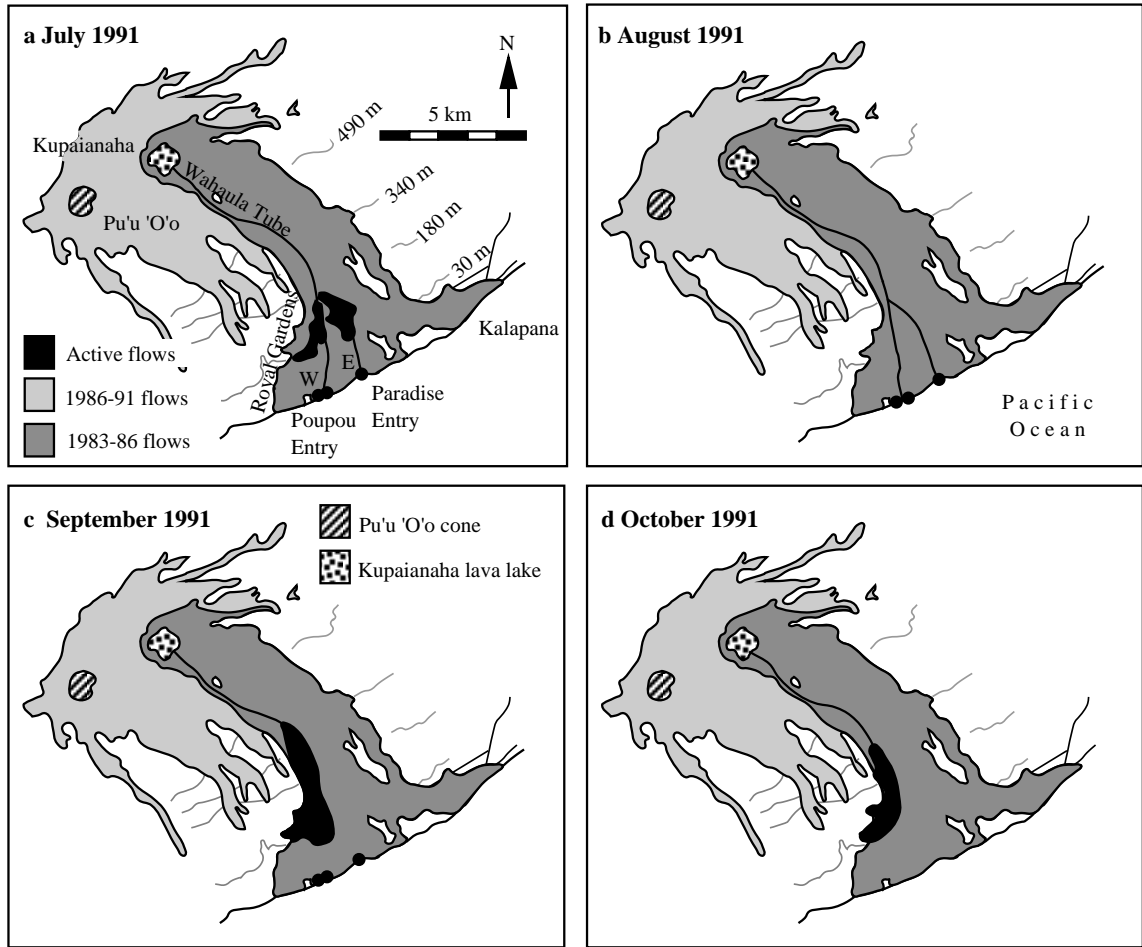


Fig. 1 Maps of the Pu'u 'O'o-Kupaianaha flow field during **a** July 1991 (GVN 1991b), **b** August 1991 (GVN 1991c), **c** September 1991 (GVN 1991d) and **d** October 1991 (GVN 1991e). These have been produced by the Hawaiian Volcano Observatory and the originals are at the referenced locations. They are reproduced here to provide a comparison for thermal maps produced from the Thematic Mapper (TM) and weather satellite (AVHRR) data (see Figs. 4, 11)

GVN 1991d). The ocean entries remained inactive, with surface breakouts from the Wahaula tube concentrated inland and on the western side of the flow field, throughout October (Fig. 1d; GVN 1991e).

Data sets

The TM data cover the visible to thermal infrared portions of the spectrum at spatial resolutions of 30–120 m (Table 1). Following Oppenheimer et al. (1993), Flynn et al. (1994), and Harris and Stevenson (1997), we processed these data to correct for atmospheric effects and to derive pixel-integrated surface temperatures in each waveband for each pixel (T_x ; Fig. 2). For TM pixels that include active lava bodies, it is common practice to assume that a pixel is occupied by two thermal components: areas of chilled crust at temperature T_c occupying fraction f_c of the pixel or lava surface, and areas

where the molten core (at temperature T_h) is exposed, this occupying $f_h (=1-f_c)$. In this case, integrated temperature T_x results from the contribution of the crusted and molten surfaces falling within the TM pixel (Fig. 2).

Following Dozier (1981), where thermal data are available at two wavebands, if any one of the three unknowns (f_c , T_c , or T_h) can be assumed, then the remaining two can be estimated by solution of simultaneous equations. For TM pixels containing active lava this has been achieved by using bands 5 and 7 with an assumed T_c (e.g., Rothery et al. 1988; Glaze et al. 1989; Pieri et al. 1990; Bhattacharya et al. 1993) or T_h (e.g., Oppenheimer 1991; Flynn et al. 1994). The assumption of a crustal temperature (T_c) can be problematic, since field measurements at active surface flows show that T_c is highly variable (Flynn and Mouginiis-Mark 1992, 1994). Erroneous selection of T_c results in large errors in calculated T_h and f_c (Oppenheimer et al. 1993, Figs. 5, 6). We therefore choose to assume T_h since it is easier to constrain.

Previous studies set T_h equal to the eruption temperature (e.g., Flynn et al. 1994), which for episode 48 was extremely stable at $1150 \pm 4^\circ\text{C}$ (Hon et al. 1993, 1994; Mangan et al. 1993, 1995; Cashman et al. 1994). However, we find that the exposed high-temperature surface is

Table 1 Landsat Thematic Mapper (TM) and Advanced Very High Resolution Radiometer (AVHRR) sensor characteristics. Min. Temp. is the minimum temperature that an isothermal surface which entirely fills a pixel must achieve to emit measurable radiance in the given waveband. Max. temp. is the temperature the surface must achieve to saturate a pixel, i.e. attain the maximum level of radiance recordable by the sensor, and are taken from Flynn et al. (1994) and Harris and Stevenson (1997)

Band	Image (swath) ^a		Repeat coverage ^b	
	Wavelength (μm)	Pixel size (m)	Min temp (°C)	Max temp (°C)
TM				
1	0.45– 0.52	30 × 30	1050	1490
2	0.52– 0.60	30 × 30	960	1410
3	0.63– 0.69	30 × 30	801	1170
4	0.76– 0.90	30 × 30	620	1000
5	1.55– 1.75	30 × 30	220	430
6	10.42–12.42	120 × 120	– 60	90
7	2.08– 2.35	30 × 30	120	290
AVHRR				
1	0.58– 0.68	1000 × 1000	800	1350
2	0.72– 1.10	1000 × 1000	500	940
3	3.55– 3.93	1000 × 1000	– 70	50
4	10.3 –11.3	1000 × 1000	–150	60
5	11.5 –12.5	1000 × 1000	–150	60

^a Swath width = 185 and 3000 km for TM and AVHRR, respectively

^b 16 days and 6 h for TM and AVHRR, respectively

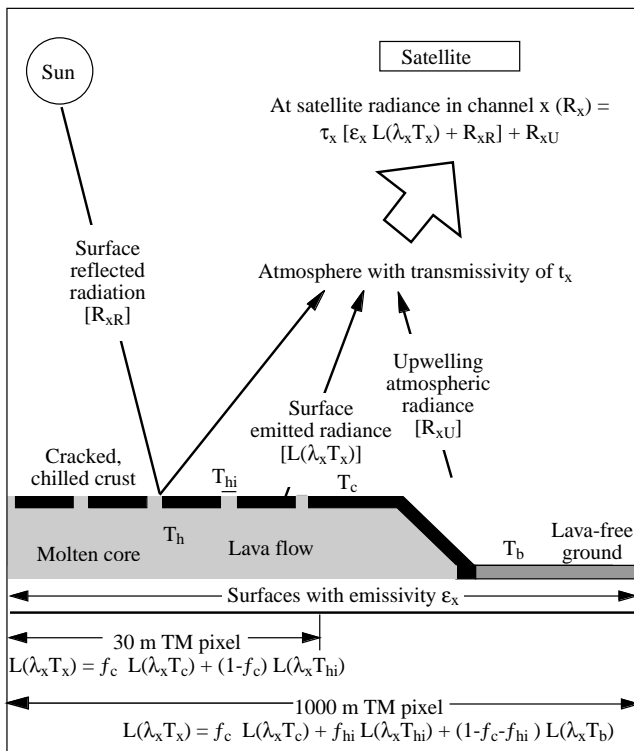


Fig. 2 Diagram showing the composition of the at-satellite radiance (R_x) for a 30-m TM and a 1000-m AVHRR pixel over an active lava. To obtain the pixel integrated temperature (T_x), all other contributions must be corrected. Note that $L(\lambda T)$ is the Planck function for a blackbody at wavelength λ and temperature T

itself an integrated temperature, which is composed of two thermal sources and is not equal to the eruption temperature. This is apparent from observations of active lava flows using a 1.1-μm video camera (L Flynn, unpublished data). These observations show a mesh of filaments forming over the incandescent surface of the

flow through which the molten core is exposed. Measurements by Flynn and Mougins-Mark (1992) show that this mesh is at a temperature of $\sim 770^\circ\text{C}$ and composes $\sim 96\%$ of the high-temperature surface; the remaining 4% is at $\sim 1150^\circ\text{C}$. This gives an integrated temperature for the hot surface of $\sim 800^\circ\text{C}$ at the TM band-5 and band-7 wavelengths. Using infrared thermometers on Kilauean's active pahoehoe flows, we have obtained temperatures for this integrated high-temperature component of between 870 and 1040°C (Fig. 3). Furthermore, infrared (0.8 – $1.1\ \mu\text{m}$) thermometer measurements of integrated temperature measurements at cracks in the surface crust where the molten interior is exposed confirm that the integrated temperatures for exposed molten surfaces are less than the eruption temperature, giving temperatures of 860 – 890°C (A. Harris, unpublished data). Therefore, to avoid error from setting the high component temperature too high, we define a new temperature variable (T_{hi}) that describes this integrated high-temperature component; we set T_{hi} to $900 \pm 100^\circ\text{C}$ (see Oppenheimer et al. 1993, Fig. 5, for error in estimates of f_c and T_c due to poor selection of T_h). This temperature component will occupy fraction f_{hi} , or $1-f_c$, of the flow surface (Fig. 2).

Although the spatial resolution of AVHRR is coarser than that of TM (Table 1), thermal data are available once every 6 h (Table 1). This greatly improves the chances of a satellite pass coinciding with a cloud-free period or short-lived phase of activity. Following Harris et al. (1997b) we assume that the larger AVHRR pixels will be occupied by a third thermal surface, lava-free ground at ambient temperatures (T_b). Hence, the pixel-integrated temperature (T_x) will result from the contribution of three thermal components: lava-free ambient ground, active lava with a chilled crust, and areas at T_{hi} (Fig. 2). We therefore use the method of Harris et al. (1997b), whereby AVHRR band-3 and band-4 data are

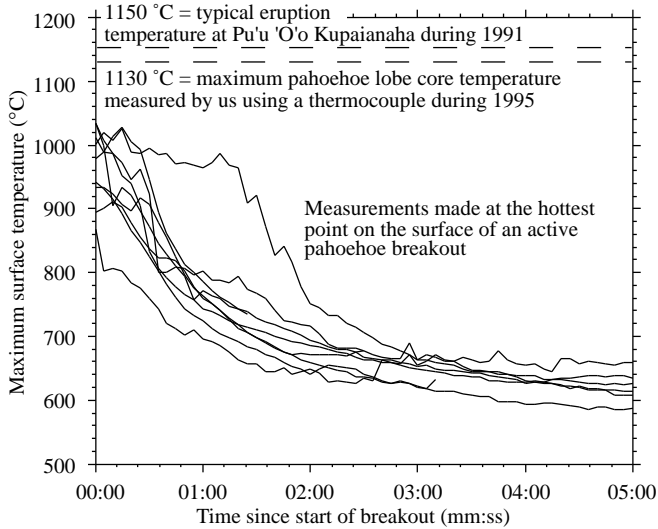


Fig. 3 Surface cooling measured during the first 5 min of emplacement at active pahoehoe breakouts at the Pu'u 'O'o-Kupaianaha lava flow field during October 1995. Temperatures were obtained using a Minolta/Land Cyclops 152 infrared ($0.8\text{--}1.1\ \mu\text{m}$) thermometer from a distance of 3–5 m, giving a field of view 14–24 cm. Data have been corrected using a spectral emissivity for basaltic pahoehoe lava of 0.925. Because of the large field of view of this instrument, measured temperatures will be an integral of the high-temperature surfaces across this field of view (T_{hi})

used with an assumed T_b and T_{hi} and a range of T_c to estimate a range of f_c and f_{hi} .

Having calculated T_c and the fraction of the flow surface at T_c (f_c), we next estimate the effective radiation temperature of the lava surface (T_e), using $T_e = [f_c T_c^4 + (1-f_c) T_{hi}^4]^{0.25}$ (Crisp and Baloga 1990; Pieri et al. 1990). Inserting T_e in the surface cooling vs time relationship given by Hon et al. (1994, Eq. (6)), we are able to estimate the mean time since the emplacement of lava within each pixel and hence the area of lava emplaced over a given period (Table 2). Using the procedures outlined in Flynn et al. (1994), we were also able to identify and measure the dimensions of lava tubes and skylights (Fig. 4; Table 2).

Model for the estimation of effusion rates using total flow-field thermal flux

Following Pieri and Baloga (1986) and Harris et al. (1997b), effusion rate (E_r) can be estimated if the total thermal flux for a moving flow (Q_{tot}) is known. Q_{tot} will equal the rate at which heat is transferred into the open flow-field system by lava flowing into and through it, and by the latent heat of crystallization, which can be written as

$$Q_{tot} = E_r \rho_{lava} [c_{plava} \Delta T_{stop} + c_L \Delta\phi], \quad (1)$$

in which ρ_{lava} and c_{plava} are the density and specific heat capacity of the lava, ΔT_{stop} is the temperature drop throughout the moving portion of the flow, $\Delta\phi$ is the mass fraction of crystals grown in cooling through

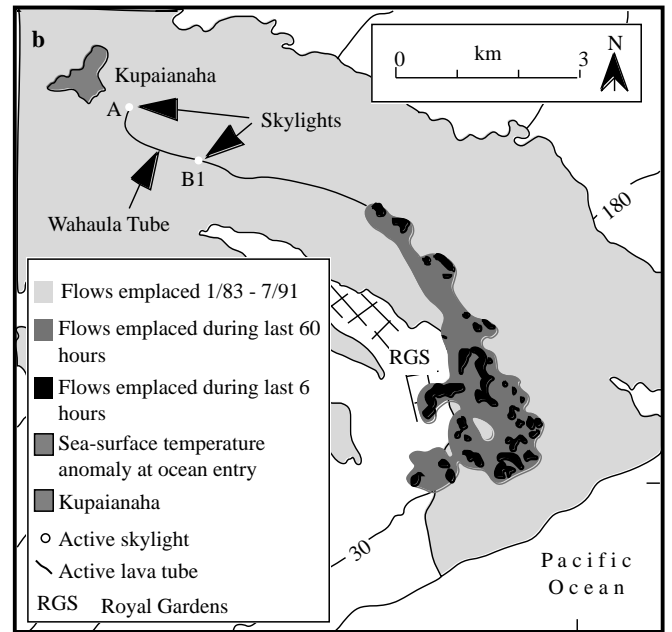
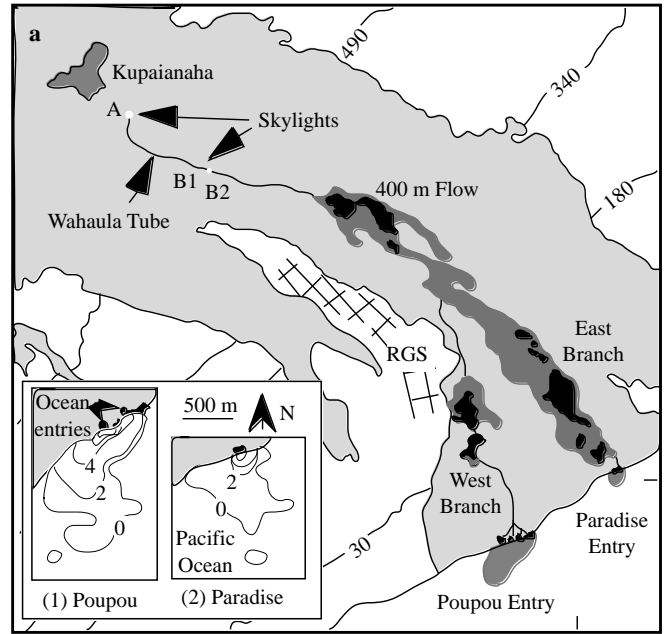


Fig. 4 Maps of the Pu'u 'O'o-Kupaianaha lava flow field made using Landsat-TM data acquired on **a** 23 July and **b** 11 October 1991. Flows emplaced since January 1983 have been mapped using bands 1–4, in which these freshly emplaced flows are evident as very low reflectance surfaces. The Kupaianaha lava lake, active tubes, skylights, and surface flows have been identified using the magnitude thresholds given in Table 3. The plume of lava-heated water off-shore of the ocean entries has been mapped using band 6-derived ocean-surface temperatures. Detail of the ocean-entry thermal plumes are *inset* in **a**, where ΔT_{water} contours are given (ΔT_{water} = plume temperature minus ambient water temperature)

ΔT_{stop} , and c_L is the latent heat of crystallization. Rearranging Eq. (1) allows E_r to be estimated from

$$E_r = \frac{Q_{tot}}{\rho_{lava} [c_{plava} \Delta T_{stop} + c_L \Delta\phi]} \quad (2)$$

Table 2 Flow field parameters estimated using Landsat-TM data acquired on 23 July and 11 October 1991

Date	23 July	11 October
Area of surface flows (km²)		
<30 ± 16 h old	4.930 ± 3.223	5.135 ± 3.474
<7 ± 2 h old	1.377 ± 0.556	2.193 ± 0.701
<2 ± 1 h old	1.117 ± 0.405	1.278 ± 0.514
<0.2 ± 0.1 h old	0.092 ± 0.004	0.058 ± 0.001
<0.1 ± 0.05 h old	0.012 ± 0.001	0.009 ± 0.001
Length of Tubed flow (m)^a		
Upper Wahaula Tube	5640 (2040)	4050 (0)
East Branch	3240 (3240)	–
West Branch	4200 (1320)	4680 (4680)
Total	13080 (6600) 8880 ^b , 9840 ^c	8730 (4680)
Skylights		
Number	3	2
Area (m ²) ^d		
A	8–11	5–7
B1	11–15	13–17
B2	5–7	
Total	24–33	18–24

^a Total length is given, with length covered by surface flows <60 h old in parentheses

^b Tube length of Upper Wahaula plus east branch

^c Tube length of Upper Wahaula plus west branch

^d See Fig. 4 for skylight locations

For vesicle-free molten Kilauea basalt, ρ_{lava} and cp_{lava} have values of $2600 \pm 100 \text{ kg/m}^3$ and 1225 J/kg K , respectively (Keszthelyi 1995a; Peck 1978). Taking into account vesicularity, which is typically 40–60% with a maximum range of 10–70% for Pu'u 'O'o–Kupaianaha lavas (Wilmoth and Walker 1993; Cashman et al. 1994), gives ρ_{lava} of $1590 \pm 840 \text{ kg/m}^3$ and cp_{lava} of $720 \pm 380 \text{ J/kg K}$. Spectroradiometer measurements of active flow fronts shows that flow motion in 'a'a and pahoehoe flows at Kilauea ceases at a temperature (T_{stop}) of $800 \pm 30 \text{ }^\circ\text{C}$ (Flynn and Mouginitis-Mark 1992). T_{stop} is a surface temperature that relates to the temperature at which the crust becomes strong enough to prevent further forward motion. However, the interior of the flow is still at higher temperatures, and forward motion may be resumed by failure or rafting up of the cooler, brittle crust to feed a new flow unit. For our study, the eruption temperature (T_{erupt}) can be set to $1150 \pm 4 \text{ }^\circ\text{C}$, which is the mean eruption temperature from measurements made during this episode of activity using the Helz and Thornber (1987) geothermometer (Mangan et al. 1993, 1995; Cashman et al. 1994) and thermocouples (Hon et al. 1993, 1994). Setting ΔT_{stop} equal to T_{erupt} minus T_{stop} gives ΔT_{stop} for this flow as $350 \pm 34 \text{ }^\circ\text{C}$. Analysis of lava samples taken from a skylight 1500 m from the vent and at surface flows 11.5 km from the vent shows a volume of crystallization of 2.2 and 4.3%, respectively, giving $\Delta\phi$ of 0.0325 ± 0.0105 for this flow (J. Kauahikaua, pers. commun.). Following previous work (Jaeger 1961; Kirkpatrick 1976; Peck et al. 1977; Shaw et al. 1977; Brandeis et al. 1984; Huppert and

Sparks 1988; Crisp and Baloga 1994) we set c_L to $3.5 \times 10^5 \text{ J kg}^{-1}$.

Determining Q_{tot} is more problematic. Pieri and Baloga (1986) set Q_{tot} equal to radiative losses, whereas Harris et al. (1997b) extended that model to include free convective losses. Recent models for tubed and surface flows (Keszthelyi 1995a; Keszthelyi and Denlinger 1996) indicate that neither of these models fully describes the heat loss from a moving lava flow. Therefore, in order to accurately constrain Q_{tot} , and thereby E_r , we construct a detailed thermal model to fully describe the heat lost by a moving flow. Some components of this model are based on thermal flux models for tubed and surface flows given by Keszthelyi (1995a) and Keszthelyi and Denlinger (1996), which used point measurements as inputs. We extend these models by estimating the total thermal flux from the entire active flow surface using the synoptic coverage afforded by remotely sensed data and ground-based measurements.

Derivation of Q_{tot} depends on the type of flow. In the most complicated case, where lava tubes feed subaerial and submarine flows, as at Kilauea during July 1991,

$$Q_{\text{tot}} = Q_{\text{tube}} + Q_{\text{surf}} + Q_{\text{ocean}}, \quad (3)$$

in which Q_{tube} , Q_{surf} , and Q_{ocean} are the thermal fluxes from the tubed, subaerial, and submarine portions of the system, respectively. If a subaerial flow is fed directly from the primary vent, with no tubed sections, the Q_{tube} term can be dropped. If lava travels from the source vent via a lava tube directly to the ocean, Q_{surf} can be neglected. Alternatively, if the flow does not enter a body of water, the Q_{ocean} term can be ignored.

Lava tubes

To define Q_{tube} we adapt the thermal model for lava tubes given by Keszthelyi (1995a), where,

$$Q_{\text{tube}} = Q_{\text{pipe}} + Q_{\text{sky}}, \quad (4)$$

in which Q_{pipe} and Q_{sky} are the thermal fluxes from lava flowing through the roofed-over (pipe) and open (skylight) portions of the lava tube, respectively (Fig. 5).

The thermal flux from the roofed portion can be described by

$$Q_{\text{pipe}} = Q_{\text{tconv}} + Q_{\text{tcond}} + Q_{\text{train}}, \quad (5)$$

in which Q_{tconv} , Q_{tcond} , and Q_{train} are the thermal fluxes from the roofed portion of the system due to convection, conduction, and rain, respectively (Fig. 5). The convective loss from a tube is given by

$$Q_{\text{tconv}} = L_{\text{tube}} \pi 0.565 \left[\frac{\rho_{\text{air}} \alpha_{\text{air}} g K_{\text{lava}} \Delta T_{\text{tube}} D_{\text{tube}}}{(\mu_{\text{air}} \beta_{\text{lava}})^{0.5} \Delta T_{\text{tube}} \kappa_{\text{lava}}} \right] \quad (6)$$

in which L_{tube} and D_{tube} are the length and diameter of the tube; g is acceleration due to gravity (9.8 m s^{-2}); ρ_{air} , α_{air} , and μ_{air} are the density, cubic expansivity, and viscosity of air; K_{lava} , β_{lava} , and κ_{lava} are the permeability,

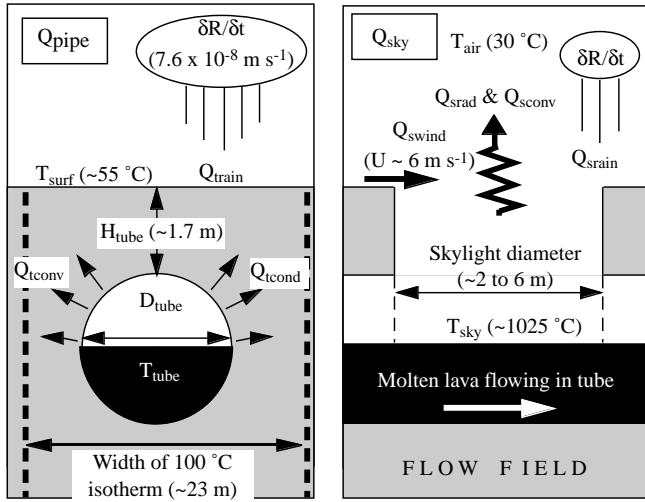
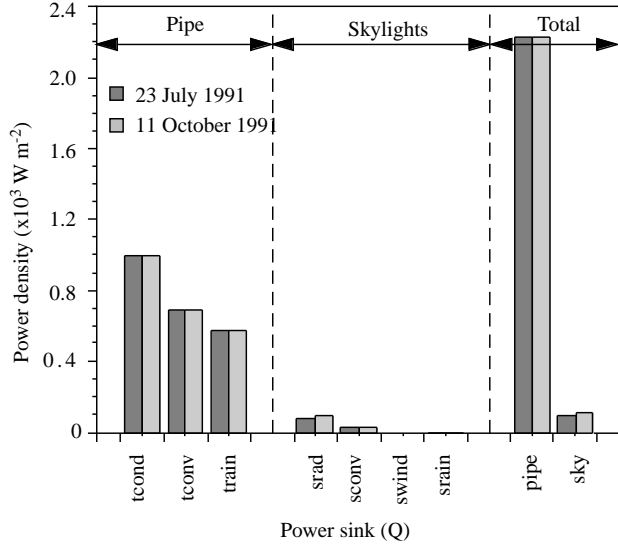


Fig. 5 *Top* Power flux in Wm^{-2} from a lava tube active under the conditions defined here for the 1991 Pu'u 'O'o-Kupaianaha eruption. Fluxes are estimated using parameters set using field observations and TM data for the flow field on 23 July and 11 October 1991. Sources of heat loss from a roofed portion of the tube system (*bottom left*) and skylights (*bottom right*) are illustrated with the variables used to calculate each flux (Eqs. (4) to (13)). Values given are typical Pu'u 'O'o-Kupaianaha tube system in 1991

thermal diffusivity, and thermal conductivity of the lava; and ΔT_{tube} is the temperature difference between the lava flowing in the tube and the surface.

We obtained L_{tube} from the TM images by tracing the master tube from Kupaianaha (Fig. 4; Table 2). Field observations have estimated tube diameters of 3–5 m, and up to 10–15 m near the vent (J. Kauahikaua, pers. commun.); hence, we use D_{tube} of 9 ± 6 m. Parameter ΔT_{tube} is calculated from T_{tube} minus T_{surf} , where T_{tube} is the temperature of lava flowing in the tube, and T_{surf} is the surface temperature above the tube. For T_{tube} at Kilauea we use the eruption temperature of 1150 ± 4 °C. Temperature T_{surf} , estimated using TM band-6 data for pixels along the course of the lava tube,

shows little variation along the length of the tube; values ranged between 59 and 61 °C and between 51 and 59 °C on the 23 July and 11 October images, respectively, giving a mean T_{surf} of 60 ± 1 °C and 54 ± 3 °C. We set ρ_{air} , α_{air} , and μ_{air} using tables in Kays and Crawford (1980) for air at a mean temperature of $(T_{\text{tube}} + T_{\text{surf}})/2$. Following Keszthelyi (1995a) K_{lava} has the value of $10^{-11 \pm 1}$ m² for basalt and κ_{lava} is calculated as a function of vesicularity using the relationship given by Peck et al. (1977) and Peck (1978), giving 1.2 ± 0.5 W/m K for the Pu'u 'O'o-Kupaianaha lavas. Thermal diffusivity is equal to $[\kappa_{\text{lava}}/(\rho_{\text{lava}} c_{p_{\text{lava}}})]$, where we use the vesicle-corrected values for each parameter.

The conductive loss from a tube can be estimated by modeling the tube as an isothermal cylinder, at temperature T_{tube} and radius r_{tube} , buried in a semi-infinite medium which has a surface temperature of T_{surf} (Holman 1992):

$$Q_{\text{tcond}} = \kappa_{\text{lava}} \Delta T_{\text{tube}} [2 \pi L_{\text{tube}} / \cosh^{-1}(H_{\text{tube}}/r_{\text{tube}})], \quad (7)$$

in which H_{tube} is the thickness of the tube roof. For this system, we can set H_{tube} at 1.7 ± 1.0 m, from the mean of the values given by Keszthelyi (1995a), and r_{tube} to 4.5 ± 3.0 m for this tube system. Observations of the crust thickness around skylights by J. Kauahikaua (HVO) show H_{tube} in these locations to be 1–2 m. However, skylights occur due to thinning of the tube roof, so that roof thicknesses in the vicinity of the skylights are probably thinner than elsewhere along the length of the tube and may thicken to as much as 3–5 m away from skylights (J. Kauahikaua, pers. commun.). We therefore regard 1.7 ± 1.0 m as a minimum value for H_{tube} .

Thermal losses due to rain from the tube system are estimated by adapting the simple model given by Keszthelyi (1995a) where,

$$Q_{\text{train}} = \partial R / \partial t A_{100} \rho_{\text{H}_2\text{O}} L_{\text{H}_2\text{O}}^+, \quad (8)$$

in which $\partial R / \partial t$ is the rainfall rate, A_{100} is the area inside the 100 °C isotherm, $\rho_{\text{H}_2\text{O}}$ is the density of water, 958 kg/m³ for water at 100 °C (Kays and Crawford 1980), and $L_{\text{H}_2\text{O}}^+$ is the latent heat of vaporization of water plus the heat needed to warm the water to 100 °C, i.e. ~ 2.8 MJ/kg (Keszthelyi 1995a). Since we are considering rain that has percolated through cracks in the flow field and is now present as groundwater, we assume that this ground water is being constantly boiled off and periodically replenished by rain at a mean rate. For this system we use the mean $\partial R / \partial t$ from Keszthelyi (1995a) of $7.6 \pm 1.7 \times 10^{-8}$ m s⁻¹. We estimate A_{100} by multiplying L_{tube} by 23 ± 9 m, the mean diameter of the 100 °C isotherm from Keszthelyi (1995a).

Following the relationships given by Hon et al. (1994), an inflating pahoehoe flow field less than 60 h old will still contain a molten core, at 1070–1150 °C, which will be up to 0.6 m thick. Active tubes beneath such areas will therefore have a layer of molten lava above them at temperatures approximately equal at those of the lava in the tube. This will effectively insu-

late the lava flowing in the tube, reducing ΔT_{tube} and the thermal flux to approximately zero. Thermal flux from the lengths of active tube beneath such recently emplaced lava is therefore zero. Thus, in the calculation of Q_{tube} , L_{tube} will equal the length of the tube system beyond flows <60 h old, i.e., 6480 and 4050 m on 23 July and 11 October 1991, respectively (Table 2).

The thermal flux from skylights can be described by

$$Q_{\text{sky}} = Q_{\text{srad}} + Q_{\text{sconv}} + Q_{\text{swind}} + Q_{\text{srain}}, \quad (9)$$

in which Q_{srad} , Q_{sconv} , Q_{swind} , and Q_{srain} are the thermal losses from the skylight due to radiation, convection, wind, and rain falling through the skylight (Fig. 5).

Radiative losses from the skylight are calculated from

$$Q_{\text{srad}} = \sigma A_{\text{sky}} T_{\text{sky}}^4, \quad (10)$$

in which ϵ is emissivity of the lava, σ is the Stefan Boltzmann constant ($5.67 \times 10^{-8} \text{ W/m}^2 \text{ K}^4$), A_{sky} is the area of the skylight, and T_{sky} is the temperature of the lava flowing through the skylight. We use ϵ of 0.9, the emissivity that we calculated from reflectance spectra for pahoehoe samples (J. Salisbury, pers. commun.) taken from, and typical of, the Pu'u 'O'o-Kupaianaha flow field. Skylight area (A_{sky}) can be calculated using the method of Flynn et al. (1994), giving values of 24–33 m² on 23 July and 18–24 m² on 11 October 1991 (Table 2). Lava flowing through skylights at Kilauea is between 900 and 1150 °C (J. Kauahikaua, unpublished data); hence, we set T_{sky} to 1025 ± 125 °C.

Convective losses from the skylight are obtained using

$$Q_{\text{sconv}} = 0.14 A_{\text{sky}} \kappa_{\text{air}} (g \alpha_{\text{air}} \rho_{\text{air}} / \mu_{\text{air}} \beta_{\text{air}})^{1/3} \Delta T_{\text{sky}}^{4/3}, \quad (11)$$

where κ_{air} , α_{air} , ρ_{air} , μ_{air} , and β_{air} are the thermal conductivity, cubic expansivity, density, viscosity, and thermal diffusivity of air, respectively. These values are taken from tables in Kays and Crawford (1980) using a mean air temperature above the skylight of $(T_{\text{sky}} + T_{\text{air}})/2$, in which T_{air} is the ambient air temperature. Our daily measurements of ambient air temperatures at the Pu'u 'O'o-Kupaianaha flow field during October 1995 give a range of 30–40 °C at sea level and 20–30 °C at an altitude of 800 m. These are similar to T_{air} of 30 °C measured during March 1993 at the same flow field by Keszthelyi and Denlinger (1996). We therefore use T_{air} of 30 ± 10 °C. Parameter ΔT_{sky} is then calculated as the difference between T_{sky} and T_{air} .

Thermal loss due to wind at the skylight is estimated from

$$Q_{\text{swind}} = U \Delta T_{\text{sky}} \rho_{\text{air}} c_{\text{p,air}} A_{\text{sky}}, \quad (12)$$

in which U is wind velocity and $c_{\text{p,air}}$ is the specific heat capacity of air, which is obtained as described for air parameters for Q_{sconv} . Our daily measurements of wind speed at the Pu'u 'O'o-Kupaianaha flow field during October 1995 give a range of 1–12 m s⁻¹, with a mean of

$6 \pm 1 \text{ m s}^{-1}$, similar to U of 3–4 m s⁻¹ reported by Keszthelyi and Denlinger (1996) in March 1993.

Thermal loss due to rain falling through the skylight is given by

$$Q_{\text{srain}} = \partial R / \partial t A_{\text{sky}} \rho_{\text{H}_2\text{O}} L_{\text{H}_2\text{O}}^+; \quad (13)$$

however, this term will only be relevant when rain is actually falling. Since we are basing our analysis on observations using cloud-free TM images, we assume that no rain is falling and therefore do not include this term in our estimation of Q_{sky} .

Surface flows

The thermal flux due to Q_{surf} is described by:

$$Q_{\text{surf}} = Q_{\text{frad}} + (Q_{\text{fconv}} \text{ or } Q_{\text{fwind}}) + Q_{\text{fcond}} + Q_{\text{frain}} + Q_{\text{fgas}}, \quad (14)$$

in which Q_{frad} , Q_{fconv} , Q_{fwind} , Q_{frain} , Q_{fcond} , and Q_{fgas} are the thermal fluxes due to radiation, free and forced convection, rain, conduction, and exsolution and escape of the gas phase, respectively (Fig. 6).

Equations (1) and (2) apply to Q_{tot} for moving lava; hence, parameters are set accordingly to calculate the thermal fluxes. For parameters obtained from the TM images this requires the identification of those pixels within which it is reasonable to expect lava to still be flowing. Our observations of active pahoehoe lobes at the Pu'u 'O'o-Kupaianaha flow field show that flows typically develop over a time span of 5–20 min (~ 0.1 – 0.3 h). After this time forward motion has usually ceased, although lobes may continue to expand through inflation (Hon et al. 1993, 1994). Therefore, in calculating Q_{surf} we use those pixels containing lava less than 0.1–0.3 h old (Table 2).

Following Oppenheimer (1991) and Harris et al. (1997b), we estimate Q_{frad} using the TM data from

$$Q_{\text{frad}} = \sum_{x=1}^n (\sigma A_{\text{pixel}} [f_{\text{cx}} T_{\text{cx}}^4 + (1 - f_{\text{cx}}) T_{\text{hix}}^4]) \quad (15)$$

in which n is the total number of pixels containing moving lava, and A_{pixel} is the area of pixel x (900 m²). Parameters f_{cx} , f_{hix} ($= 1 - f_{\text{cx}}$), T_{cx} , and T_{hix} are the fractions and temperatures of the crusted and integrated high-temperature components occupying pixel x . These parameters are estimated by applying the methods and assumptions given by Flynn et al. (1994) on a pixel-by-pixel basis. In this study, T_{hix} is set at 900 ± 100 °C and T_{cx} , f_{cx} , and f_{hix} are calculated using TM bands 5–7 (Flynn et al. 1994). The resulting T_{cx} , f_{cx} , and f_{hix} range from 126 to 425 °C, 0.99998 to 0.998 and 1.9×10^{-5} to 1.95×10^{-3} , respectively.

We estimate Q_{fconv} by assuming that free convection occurs from a surface at T_e through a thermal boundary layer at T_{bound} , to ambient air at T_{air} . In this case

$$Q_{\text{fconv}} = \sum_{x=1}^n (0.14 A_{\text{pixel}} \kappa_{\text{air}} [g \alpha_{\text{air}} \rho_{\text{air}} / \mu_{\text{air}} \beta_{\text{air}}]^{1/3} \Delta T_f^{4/3}) \quad (16)$$

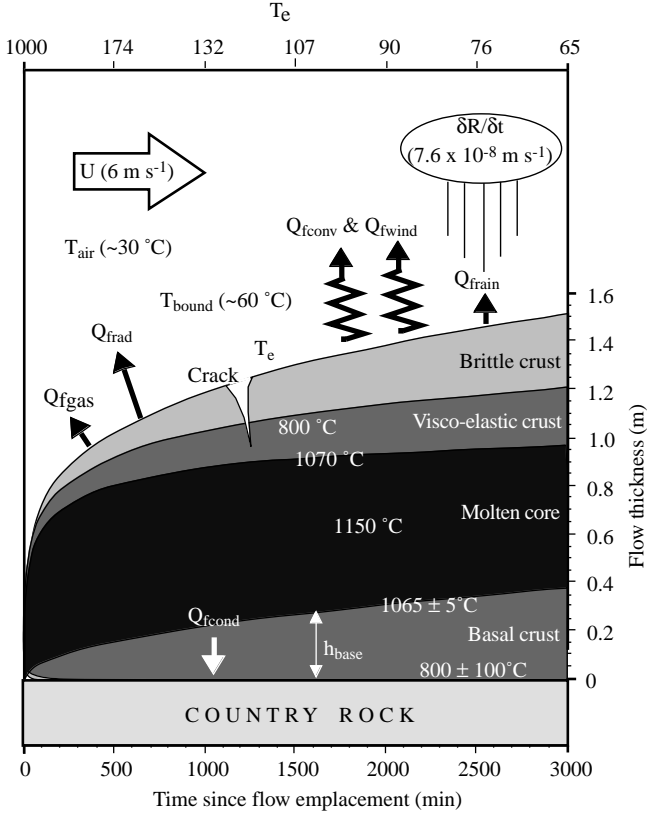


Fig. 6 Diagram illustrating heat loss from an active pahoehoe lobe, with the variables used to calculate each flux (Eqs. (14) to (20)). Values given are typical Pu'u 'O'o-Kupaianaha tube system in 1991. The pahoehoe lobe is cooling (top x -axis) and thickening (y -axis) with time (bottom x -axis). The relationships between time, effective surface temperature (T_e), and the thickness of the core, and the brittle, visco-elastic, and basal crusts are calculated following Hon et al. (1994)

in which, for TM pixel x , $\Delta T_f = T_e - T_{\text{air}}$. Over-active surface flows, κ_{air} , α_{air} , ρ_{air} , μ_{air} , and β_{air} have typically been set for stagnant air using air at T_{bound} equal to $(T_e + T_{\text{air}})/2$ (e.g., Head and Wilson 1986; Oppenheimer 1991; Harris et al. 1997b).

Following Arya (1988) we calculate Q_{fwind} using

$$Q_{\text{fwind}} = \sum_{x=1}^n (A_{\text{pixel}} C_H U \rho_{\text{pair}} c_{\text{pair}} \Delta T_f) \quad (17)$$

in which C_H is $(U^*/U)^2$, where U^* is the friction wind speed. Parameter (U^*/U) has been measured by Greeley and Iversen (1987) as ~ 0.06 at the Amboy lava field (Mojave Desert, USA). However, in this case, due to the presence of wind, the relationship used for Eq. (17) to calculate T_{bound} will not apply. Our measurements of T_{bound} in non-stagnant air over active pahoehoe flows show that setting $T_{\text{bound}} = (T_e + T_{\text{air}})/2$ will set T_{bound} too high (Fig. 7). In Eq. (17) we therefore set T_{bound} using the relationship obtained from applying a linear best-fit to the data set given in Fig. 7. Thermal parameters for air are then set from tables in Kays and Crawford (1980) using a T_{bound} of $42.605 + 0.06103T_e$

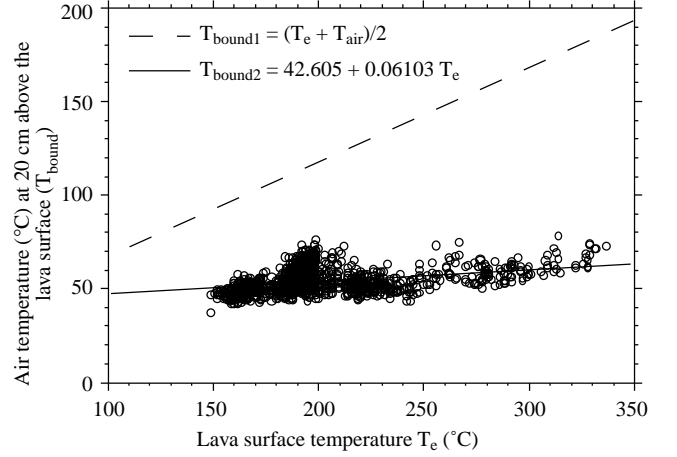


Fig. 7 Boundary-layer air temperature (T_{bound}) for non-stagnant air over an active pahoehoe lobe with a surface at temperature T_e . Calculated and measured values of T_{bound} are given. $T_{\text{bound}1}$ (dashed line) is calculated from the relationship for stagnant air $(T_e + T_{\text{air}})/2$, in which T_{air} is the ambient air temperature at 35°C (this is T_{air} at the time of our field measurements of T_{bound}). $T_{\text{bound}2}$ (open circles) gives boundary-layer air temperatures measured in the field above cooling pahoehoe lobes at the Pu'u 'O'o-Kupaianaha lava flow field during October 1995. These measurements were made at a height of 20 cm above the surface using a K-type thermocouple mounted on a static thermocouple stand. Simultaneous temperature measurements were made for the lava surface directly below the thermocouple using a static, tripod-mounted Minolta/Land Cyclops 330 infrared ($8\text{--}14\ \mu\text{m}$) thermometer from a distance of 5 m, giving a 30-cm field of view. These data have been corrected using an 8- to $14\text{-}\mu\text{m}$ emissivity for basaltic lava of 0.95. The data set consists of 1326 measurements made over three periods lasting 30, 210, and 240 min, respectively. The solid line gives the linear best fit to the $T_{\text{bound}2}$ field data

(Fig. 7). We also note that, following Keszthelyi and Denlinger (1996), Eq. (17) may underestimate Q_{fwind} by a factor of up to 5–7.

Free- (Q_{fconv}) and forced- (Q_{fwind}) convection cannot occur together: Q_{fconv} will occur only if wind speeds are sufficiently small (Head and Wilson 1986). Therefore, following Wilson and Head (1994), we use whichever is the greater of Q_{fconv} and Q_{fwind} in estimating Q_{surf} (Eq. (14)).

Thermal flux Q_{fcond} is obtained from

$$Q_{\text{fcond}} = \sum_{x=1}^n (A_{\text{pixel}} \kappa_{\text{lava}} [\Delta T_{\text{base}}/h_{\text{base}x}]) \quad (18)$$

in which ΔT_{base} is the temperature difference between the top and bottom of the basal crust and $h_{\text{base}x}$ is the thickness of the basal crust for the active flow in pixel x (Fig. 6). We set ΔT_{base} using a temperature for the top of the basal crust of $1065 \pm 5^\circ\text{C}$, the temperature measured at the core-crust contact in Hawaiian lava lakes (Peck et al. 1966; Wright and Okamura 1977; Peck 1978), and a bottom temperature of $800 \pm 100^\circ\text{C}$, typical of those measured by Keszthelyi (1995b) 1–20 min after emplacement. The thickness of the basal crust is estimated on a pixel-by-pixel basis using the pixel T_e in

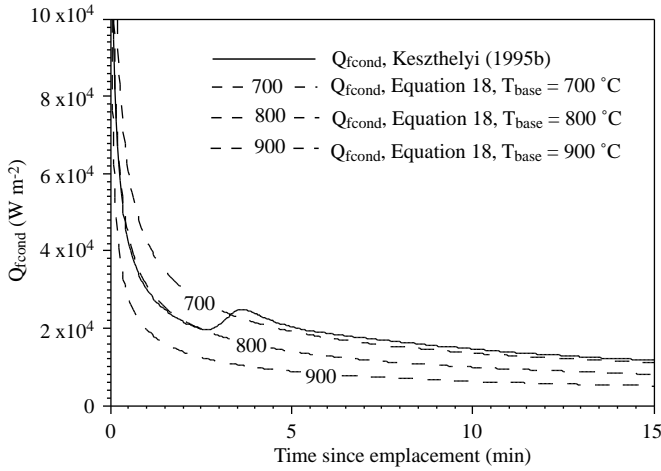


Fig. 8 Q_{fcond} as a function of time calculated from field measurements (Keszthelyi 1995b) and using Eq. (18). Equation (18) has been run using a temperature at the bottom of the basal crust (T_{base}) of 800 ± 100 °C, with a basal crust that thickens with time according to the relationships given by Hon et al. (1994)

the relationship between temperature, time, and crustal thickness given by Hon et al. (1994; Fig. 6.) This approximation of Q_{fcond} gives a conductive thermal flux which is similar to those derived from field measurements of basal cooling by Keszthelyi (1995b; Fig. 8).

Fluxes Q_{frain} and Q_{fgas} are obtained using the total lava flow area estimated TM data, A_{flow} (Table 2), in

$$Q_{frain} = \partial R / \partial t A_{flow} \rho_{H_2O} L_{H_2O} \quad (19)$$

and

$$Q_{fgas} = F_{gas} c_{p_{gas}} \Delta T_{gas} + F_{H_2O} L_{H_2O}, \quad (20)$$

in which F_{gas} and $c_{p_{gas}}$ are the flux and specific heat capacity of gas released by the active flows, respectively, with the latter having a value of $1600 \text{ J kg}^{-1} \text{ K}^{-1}$ for a mixture of CO_2 and H_2O at 700 K. Parameter ΔT_{gas} is the cooling of the gas from magmatic (~ 1150 °C) to ambient (~ 30 °C) temperatures (i.e., 1120 °C), F_{H_2O} is the flux of water vapor from the active flows, and L_{H_2O} is the latent heat of water condensation ($2.26 \times 10^6 \text{ J kg}^{-1}$). Using the surface-degassing flux and gas composition measurements given by Cashman et al. (1994) for the Pu'u 'O'o-Kupaianaha flows, we obtain F_{gas} and F_{H_2O} of 0.14 and 0.12 kg s^{-1} , respectively, for an average lava flux $\sim 1.7 \text{ m}^3 \text{ s}^{-1}$. Since the TM images that we are using are cloud free, we assume that rain was not falling at the time of image acquisition. Therefore, as with Q_{srain} , we do not include the Q_{frain} term in our estimation of Q_{surf} .

Ocean-entry flows

Heat lost by lava flowing into water (Q_{ocean}) is given by:

$$Q_{ocean} = Q_{water} + Q_{vap}, \quad (21)$$

in which Q_{water} is the heat required to raise the temperature of the water body and Q_{vap} is the heat lost by the vaporization of water (Fig. 9). We describe the former using

$$Q_{water} = (\rho_{water} c_{p_{water}} \Delta T_{water} V_{water}) / R. \quad (22)$$

In this case ρ_{water} and $c_{p_{water}}$ are the density and specific heat capacity of seawater, 1020 kg m^{-3} and $4005 \text{ J kg}^{-1} \text{ K}^{-1}$, respectively, for water temperatures of 30 – 40 °C (typical of the lava-heated water off-shore of this flow field; Sansone and Resing 1995). Parameter ΔT_{water} is the temperature difference between the water within the plume heated by the submarine flows and the surrounding non-heated water at ambient temperatures. V_{water} is the volume of water heated by ΔT_{water} (Fig. 9). We calculate ΔT_{water} using TM band-6 data to estimate the temperature of the warm-water plume (T_{plume}) and ambient, unheated sea-surface temperatures (T_{ocean}), i.e., $\Delta T_{water} = T_{plume} - T_{ocean}$, with ΔT_{water} having a value of 1 – 20 °C for this plume (Appendix A). Parameter R is the residence time of the water within a known area or the time that a parcel of water takes to travel a known distance. This is defined by $R = L_{water} / C_v$, in which C_v is the current velocity and L_{water} is the distance across the known area in the current direction. Off-shore of the active flows at Kilauea, C_v is typically 0.05 m s^{-1} . R is 600 s because we set L_{water} equal to the length of a TM pixel (30 m).

Measurements by Sansone and Resing (1995), using a thermister lowered from a boat through the plume, show that the ocean-surface thermal anomaly affects only the top 1–3 m of water. This thickness also shows variation with temperature, plumes at ΔT_{water} of >15 and ≤ 15 °C typically having thicknesses of 0.5–1.5 m and 1–3 m, respectively (Sansone and Resing 1995). We therefore estimate V_{water} using a thickness of 1 ± 0.5 m for pixels with $\Delta T_{water} > 15$ °C and 2 ± 1 m for pixels with $\Delta T_{water} \leq 15$ °C. Using the heated water plume identified in the July TM image (Fig. 4a) and a typical thickness of 2 ± 1 m gives a total volume of heated water of 1.6×10^6 and $7.8 \times 10^5 \text{ m}^3$ and Q_{water} of 4.96 and 2.07 GW for the Poupou and Paradise entries, respectively, or a total of 7.03 GW. All estimates have errors of $\pm 50\%$. Our estimates for Q_{water} are consistent with estimates for total Q_{water} based on in situ plume temperature measurements made during mid-1989 and April 1991, respectively, of 2.0–3.5 and 7.0 GW (Resing 1997).

We estimate Q_{vap} from

$$Q_{vap} = (\rho_{water} L_{H_2O} + V_{vap}) / R, \quad (23)$$

in which V_{vap} is the volume of water vaporized. Field measurements of the heated water plume off-shore of the Pu'u 'O'o-Kupaianaha flows during 1989 and 1991 show a 1% increase in salinity within the plume (Resing 1997). This indicates that 1% of the total water volume heated by ΔT_{water} is being vaporized, i.e.,

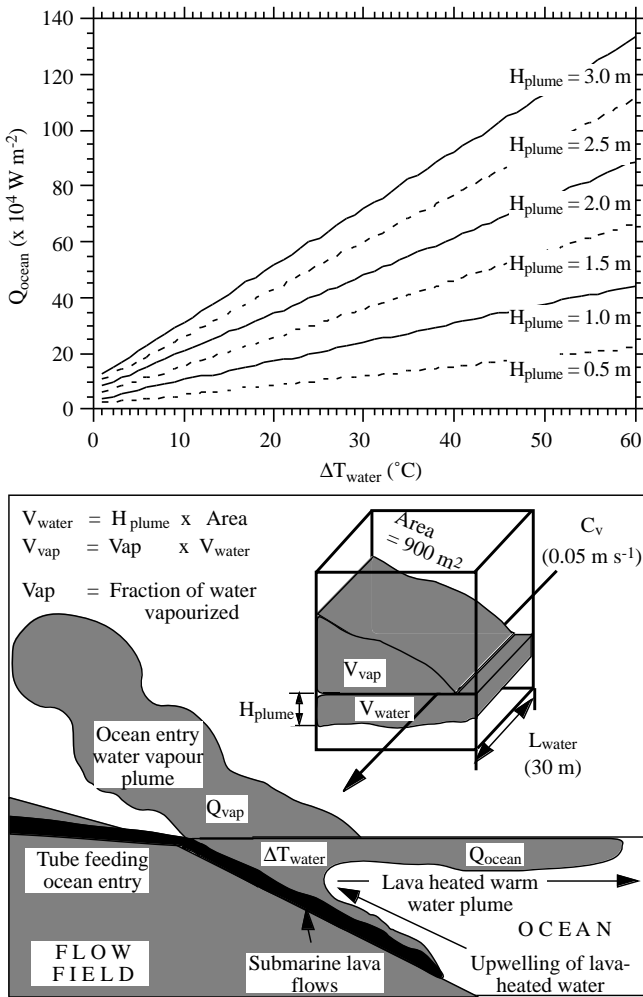


Fig. 9 *Top* Relationship between Q_{ocean} and ΔT_{water} for several plume thicknesses (H_{plume}) typical of the lava-heated warm-water plume off-shore of the Pu'u 'O'o-Kupaianaha lava flow field. *Bottom* Diagram showing the sources of heat loss, and the variables used to calculate them (Eqs. (21) to (23)), for a lava flow entering a water body

$V_{\text{vap}} = 1\%$ of V_{water} . This gives V_{vap} of $9 \pm 4.5 \text{ m}^3$ per pixel.

Discussion of flow-field activity and effusion rates

Using the characteristic size, shape, and form of various eruption features in TM thermal data described by Flynn et al. (1994), we examined the two TM images to identify, measure, and map active features within the flow field. Analysis of the distribution of thermal anomalies in images reveals several areas of surface flows fed by tube systems, which in the 23 July 1991 image extended to the coast (Fig. 4).

Herein we also develop Flynn et al.'s (1994) use of "magnitude" as "the relative abundance of the radiative flux from the anomaly when compared with that of

non-anomalous pixels," to analyze the flow-field anomaly. Areas of active and recently active lava on both TM images cause anomalous zones of elevated radiance. Within this anomalous area we define six radiance zones based on the magnitude of the flux within each zone (Table 3). For each zone we estimated the mean effective temperature (T_e) of the flow surface. Using T_e in the surface cooling vs time relationship given by Hon et al. (1994, Eq. (6)) we were able to estimate the mean time since emplacement for flows within each magnitude zone (Table 3). From Table 3 it is apparent that zones with higher magnitudes are occupied by flow surfaces with higher effective temperatures and lower ages.

The tube system

In both images the tube system can be traced as a sinuous line of low-magnitude pixels extending from a location $\sim 360 \text{ m}$ south-southeast of the Kupaianaha lava lake, itself identifiable as a zone of low-magnitude pixels (Fig. 4; Table 3). This indicates Kupaianaha as the source of the tube system. Indeed, these anomalies are the result of the active Wahaula tube system extending from the Kupaianaha vent (Fig. 1; GVN 1990a, b, 1991a–e). High-magnitude pixels at points along the tube system locate two to three skylights (Fig. 4). Our image-based skylight-area estimates given in Table 2 and obtained using the method of Flynn et al. (1994) agree with field estimates of $5\text{--}10 \text{ m}^2$ per skylight (J. Kauahikaua, pers. commun.).

The contribution of Q_{sky} to Q_{tube} depends on the total area of the skylights; the greater the area of skylights per unit length ($A_{\text{sky}}/L_{\text{tube}}$), the greater will be the contribution of Q_{sky} . Using A_{sky} and L_{tube} calculated using the TM data, $A_{\text{sky}}/L_{\text{tube}}$ for this tube system is $\sim 0.01 \text{ m}^2/\text{m}$ on 23 July and 11 October, resulting in an identical percent contribution from Q_{sky} to Q_{tube} on both dates (Fig. 10). In terms of the total thermal loss from this tube system and total flow-field system, we find that losses due to Q_{sconv} , Q_{swind} , and Q_{srain} are trivial (Fig. 10). This is in agreement with Keszthelyi (1995a) who found the contribution of Q_{sky} to be negligible.

Our estimates for thermal flux density, i.e., total thermal flux divided by the area over which that flux occurs, from this active tube system, along with the typical values of variables used for this tube system are given in Fig. 5. Total thermal flux from the entire active tube systems feeding the Pu'u 'O'o-Kupaianaha flow field on 23 July and 11 October 1991 is given in Fig. 10. Our estimate for total thermal flux density for the active tube system of $2.2 \times 10^4 \text{ W m}^{-2}$ is in agreement with the value of $\sim 2.4 \times 10^4 \text{ W m}^{-2}$ estimated for this tube system by Keszthelyi (1995a) and translates to a cooling rate within the lava tube of $\sim 1 \text{ }^\circ\text{C km}^{-1}$. This is consistent with direct field measurements (Helz et al. 1991).

Table 3 Magnitude zones and threshold applied to define each zone on the 23 July (23/7) and 11 October (11/10) 1991 TM images, with the number of pixels, mean effective temperature (T_e) and age or time since emplacement for lava within each zone. DN_x is the pixel digital number in band x , B_x is the background DN in channel x (we use the mean and standard deviation of ~ 5500 non-anomalous pixels) and SAT is saturation, i.e. the highest recordable DN. Note that (1) Band 6 can detect radiance from surfaces at temperatures higher than -60°C , but bands 7 or

5 will not detect radiance until a surface has reached 120 or 220°C respectively; and (2) band 7 is more sensitive than band 5 to typical active lava temperatures. Given a pixel occupied by ambient ground at 45°C and lava at 900°C , lava must occupy $\sim 3\%$ of a band 7 pixel in order to saturate, yet a band 5 pixel would not saturate until lava occupied $\sim 17\%$. Therefore, our thresholds become increasingly “tight”, i.e. pixels must be increasingly “hot” to pass thresholds (1) to (6)

Magnitude	Threshold description	No. of pixels		Mean T_e ($^\circ\text{C}$)		Age (h)	
		23/7	11/10	23/7	11/10	23/7	11/10
1 Low	$DN_6 > B_6 + 5$	680 ± 444^a	432 ± 134^a	97 ± 27	114 ± 18	30 ± 9	22 ± 6
2 Low-moderate	$DN_7 > B_7 + 5$	1530 ± 618	2347 ± 779	198 ± 15	193 ± 13	6 ± 1	6 ± 1
3 Moderate	$DN_5 > B_5 + 5$	1241 ± 450	1420 ± 571	266 ± 8	248 ± 14	2 ± 0.2	2.5 ± 0.5
4 Moderate-high	$DN_7 = \text{SAT};$ $DN_5 = B_5 + 100$	102 ± 5	64 ± 1	392 ± 2	385 ± 2	0.2 ± 0.01	0.3 ± 0.01
5 High	$DN_7 = \text{SAT};$ $DN_5 = B_5 + 100$	26 ± 1	10 ± 1	416 ± 1	418 ± 1	0.2 ± 0.01	0.2 ± 0.01
6 Very high	$DN_5 + DN_7 = \text{SAT}$	13	1	>425	>425	<0.1	<0.1

^a Count for $120 \times 120\text{-m}$ band-6 TM pixels; all other counts are for $30 \times 30\text{-m}$ band-5 or band-7 pixels (see Table 1)

Active lava flows

In Fig. 4 mapped flows emplaced within 6 and 60 h of image acquisition are shown. On the 23 July image, we note three main areas of 6-h-old flows: (a) flows at 400 m elevation; (b) an eastern flow zone; and (c) a western flow zone (Fig. 4). These areas are surrounded by a larger area of flows up to 60 h old. The flows at 400 m elevation issue from the master tube, which bifurcates at an elevation of ~ 180 m, beneath the zone of 60-h-old flows. The western branch feeds the western flow zone and enters the sea at the Poupou ocean entry, and the eastern branch feeds the eastern flow zone, entering the sea at the Paradise ocean entry (Fig. 4a). The thermal distribution resulting from the higher (~ 400 m elevation) flows and the lower (10–100 m elevation) flows is also apparent in a thermal map produced using AVHRR data acquired on the same day (Fig. 11a). However, the lack of anomalous radiance between the 340 and 490 m elevation on all subsequent AVHRR thermal maps indicates that the higher flow had become inactive by 14 August (Fig. 11). This is consistent with an absence of thermal radiance in this area on the 11 October TM image (Fig. 4b) and the interpretation by Flynn et al. (1994) that radiant flux density emitted by the 400 m elevation flows indicated waning surface activity. This is evident on Fig. 4a from the larger low-magnitude (light-gray) zone surrounding the high-magnitude (dark-gray) zone. We interpret the lower-magnitude zone as resulting from cooler, stationary, but possibly still-inflating flow units emplaced during a period of more extensive surface activity between 6 and 60 h before this image was acquired.

By 11 October we note a shift in the main zone of active flows from the central flow field area to the western edge. Westward transition of the active flow zone has resulted in the inundation of land previously un-

touched by this eruption within the Royal Gardens subdivision (Fig. 4b). These developments are also apparent from thermal maps produced from the AVHRR time series, with zones of highest radiance overlapping the western flow field margin from mid-August through mid-October (Fig. 11), and are confirmed by ground observations (compare Figs. 1, 4, 11), which show surface flows extending beyond the western margins of the pre-existing flow field during August and September (Fig. 1c; GVN 1991c, d). Flows destroyed two of the remaining houses in the Royal Gardens subdivision approximately 2 weeks after the October TM image was acquired (GVN 1991e).

The frequency distribution for the temperature of, and the pixel fraction occupied by, the crust (T_c and f_c) calculated from the TM data show nearly identical frequency distributions on both dates (Fig. 12). Our calculated T_c and f_c show that crust with temperatures of $150\text{--}250^\circ\text{C}$ typically occupy $>99.98\%$ of the flow surface. Measurements by Hon et al. (1994) show that an active pahoehoe field can continue inflating for up to 350 h after flow emplacement. We suggest that our frequency distribution is dominated by inflating units almost totally covered with crustal material at T_{hi} being exposed at cracks occupying $<0.02\%$ of the surface. The remaining pixels in the tail of Fig. 12b, with lower crustal coverage (99.80–99.97%), may be due to pixels occupied by active breakouts and forward-moving lava flow units. At such pixels the increased exposure of high-temperature material (now covering 0.03–0.2% of the surface) would be explained by ruptures and tears in the crust at the active breakouts. We speculate that such frequency distributions may be a means of distinguishing pahoehoe and ‘a’a flows. The different crustal characteristics of the two flow-field types, the pahoehoe field dominated by uniformly crusted inflating lobes and the ‘a’a flow characterized by channels covered by

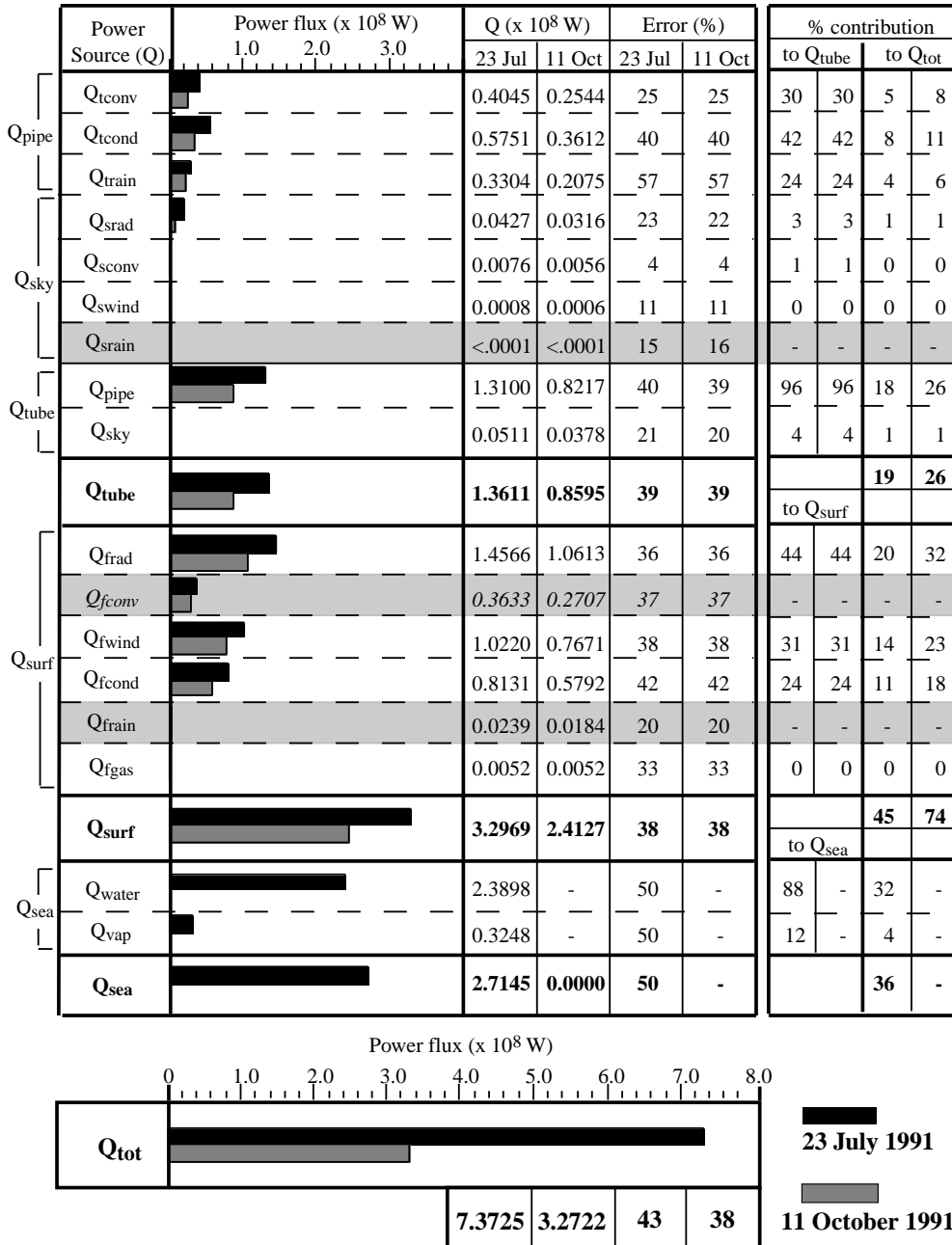


Fig. 10 Heat fluxes calculated, with percent error on each value, for the Pu'u 'O'o-Kupaianaha lava flow field on 23 July and 11 October 1991. The percent contribution of each flux both to the relevant sub-flux (Q_{tube} , Q_{surf} , and Q_{sea}) and the total flux (Q_{tot}) is given for both dates. Fluxes marked by *gray shading* are not included in Q_{tot} . Since free (Q_{fconv}) and forced (Q_{fwind}) cannot occur together, only the dominant convective flux (i.e., Q_{fwind}) is included in Q_{tot} . Q_{srain} and Q_{frain} are also not included since rain was not falling at the time of measurement. (N.B. $Q_{sea} = Q_{ocean}$)

a discontinuous crust of clinker, would reasonably result in different frequency distributions for T_c and f_c .

Previous models describing the thermal flux from surface lava flows have assumed, but not proven, that the contribution of Q_{fcond} is negligible (e.g., Danes

1972; Oppenheimer 1991; Harris et al. 1997b). However, our model shows that Q_{fcond} is not negligible (Fig. 10). During the first few seconds of emplacement, when the basal crust is very thin, Q_{fcond} dominates over all other heat fluxes (Fig. 13). By approximately 6 s after emplacement, thickening of the basal crust results in a decrease in the relative contribution of Q_{fcond} to Q_{surf} . However, Q_{fcond} contributes 15–40% of Q_{surf} during the first 10 min of flow emplacement and 10–30% thereafter (Fig. 13). This is consistent with the relationships given by Hon et al. (1994), which give basal crusts that are 33% of the total flow thickness during pahoehoe lobe cooling (Fig. 6). We therefore suggest that Q_{fcond} cannot be ignored if this thermal model is applied to a pahoehoe flow. Our observations of Hawaiian 'a'a flows

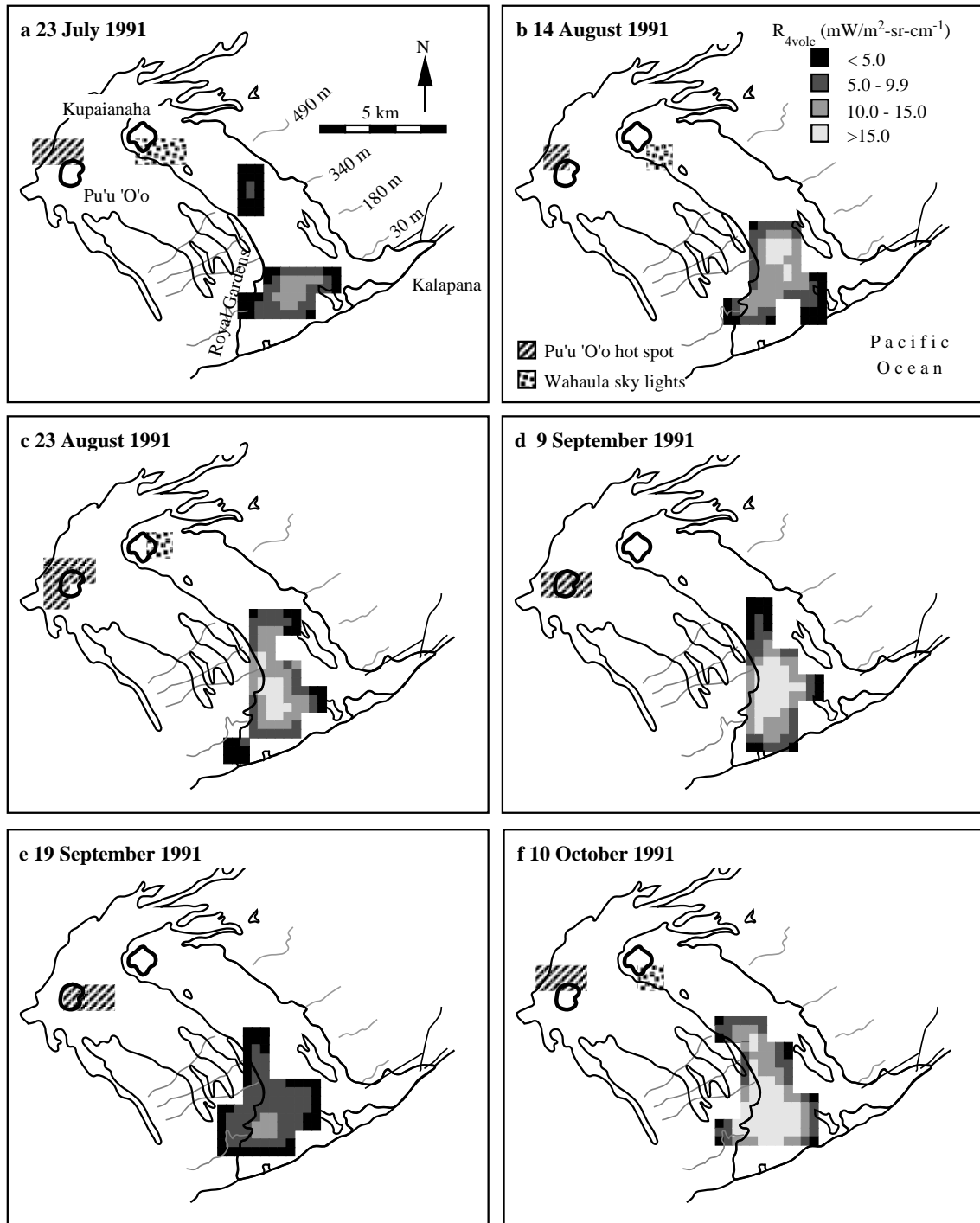


Fig. 11 Thermal maps of the Pu'u 'O'o-Kupaianaha lava flow field made using AVHRR data acquired between July and October 1991. We map R_{4volc} , the amount by which the presence of active lava in a band-4 pixel has elevated the band-4 radiance for that pixel above that of the ambient background. Pixels were re-sampled using the technique given by Harris et al. (1995, 1997a) and fitted to a map of the Pu'u 'O'o-Kupaianaha flow field using Pu'u 'O'o and Kupaianaha as tie points

give basal crusts which represent 10–30% of the total flow thickness. For a typical 'a'a flow with a thickness of 1 m, and a hypothetical basal temperature of $600 \pm 300^\circ\text{C}$, Q_{fcond} contributes 10–30% of the total thermal flux (Q_{surf}) during the first 2 h of 'a'a flow emplacement. Thus, we also suggest that Q_{fcond} cannot be ignored if this thermal model is applied to an 'a'a flow. However, fluxes Q_{frain} and Q_{fgas} are trivial and their contributions to Q_{surf} can safely be assumed to be insignificant (Fig. 10).

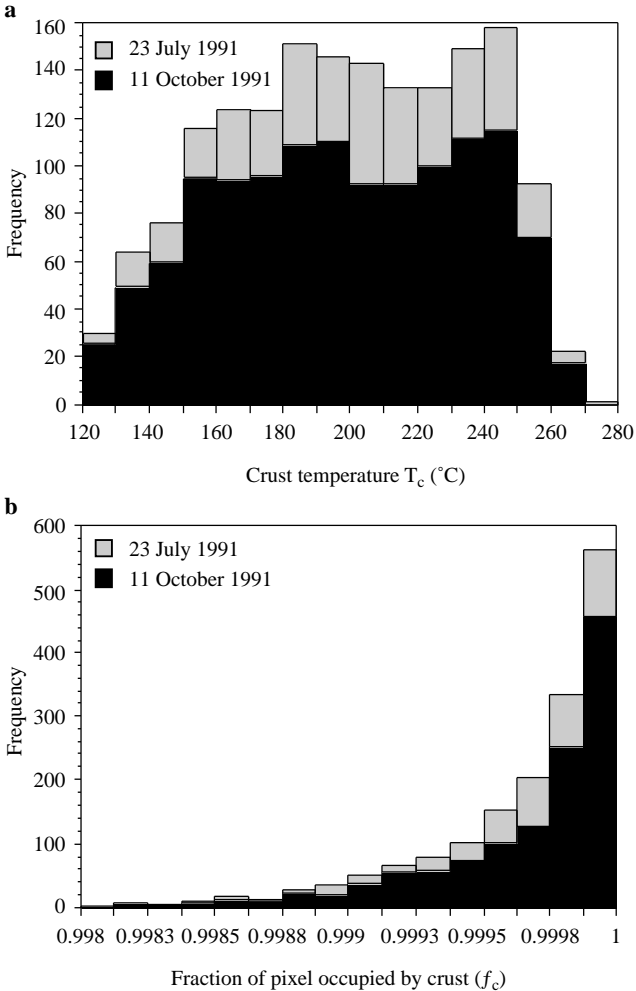


Fig. 12 **a** Frequency distribution for crustal temperatures (T_c) and **b** the fraction of a pixel occupied by crust at T_c calculated on a pixel-by-pixel basis using the 23 July and 11 October TM images

Ocean entry

The 23 July TM image shows that both the west and east branches of the Wahaula tube reach the sea, where ocean-entry sites are apparent as high-magnitude thermal anomalies in bands 5 and 7 (Fig. 4a). However, the 11 October TM image shows no ocean entries (Fig. 4b). Ground observations show a western tube establishing during August and October 1990 (GVN 1990b) that fed the Poupou ocean entry until 20 September 1991 (GVN 1991d). The eastern tube was established during April 1991 and eventually fed the Paradise entry (GVN 1991a), which became inactive on 3 September 1991, when “numerous breakouts and surface flows apparently reduced lava supply to the ocean entry” (GVN 1991d).

Off-shore of the Poupou and Paradise ocean entries on the 23 July TM image, we observe two thermal anomalies in band 6, within which ocean-surface tempera-

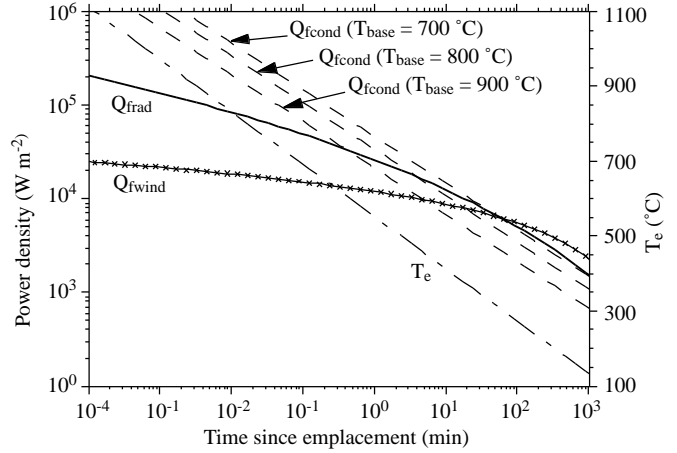


Fig. 13 Q_{fwind} , Q_{frad} , Q_{fcond} , and T_c as a function of time, where T_c has been estimated using the relationships given by Hon et al. (1994) and parameters typical of pahoehoe lobes at Pu'u 'O'o-Kupaianaha lava flow field during 1991 (Eqs. (15) to (18); Fig. 6). Q_{fcond} has been calculated using T_{base} of 800 ± 100 °C, with a basal crust which thickens with time according to the relationships given by Hon et al. (1994)

tures are elevated by between 1 and 8 °C (defined as ΔT_{water}) above the surrounding ambient ocean-surface temperatures (Fig. 4a). The two thermal plumes extend between 1200 and 800 m off-shore, covering an area of 7.8×10^5 and 3.9×10^5 m^2 , at the Poupou and Paradise entries, respectively. This compares well with ~ 1200 m seaward extension of the thermal plume observed by Sansone and Resing (1995, Fig. 2f) during March 1991. However, Sansone et al. (1991) measure maximum ΔT_{water} of up to 43 °C. Using band-6 pixels which are entirely filled by ocean, we observe a maximum ΔT_{water} of just 8 °C. This is because the maximum temperatures occurred within ~ 100 m of the shore and therefore within mixed land/ocean pixels not considered using this approach. Therefore, to estimate the maximum ΔT_{water} within such mixed coastal band-6 (120-m) pixels, we apply the mixture modeling technique given in Appendix A. This approach gives maximum ΔT_{water} of 14–20 °C and 17–19 °C at the Paradise and Poupou entries, respectively, with maximum ΔT_{water} occurring within 30 m of the shore. This compares well with a mean ΔT_{water} of 20 °C obtained from in situ temperature measurements between 1989 and 1991 (Sansone and Resing 1995). To assess the accuracy of our results, we also applied the approach of Appendix A to mixed coastal pixels containing water at ambient temperatures. The TM image shows ambient ocean-surface temperatures to be nearly uniform off-shore of the Pu'u 'O'o-Kupaianaha flow field. This enabled us to assess the accuracy of the method by comparing ocean-surface temperature calculated from mixed land–ocean pixels with that expected from adjacent pixels fully occupied by ocean. Testing the method on 20 mixed coastal pixels gave ocean-surface temperature to within 0.3–3.7 °C

of the temperature expected from off-shore ocean filled pixels. We therefore expect similar accuracy when applying this approach to plume pixels.

Our results show that Q_{ocean} will vary between 5×10^4 and $1.35 \times 10^6 \text{ W m}^{-2}$ depending on the depth and magnitude of the temperature anomaly (Fig. 9). At ocean surfaces and crater lakes, differences of 0.1–1.5°C have been found between the surface temperature and the bulk temperature (Paulson and Simpson 1981; Schluessel et al. 1990; Oppenheimer 1997). Since our measurements are of the ocean-surface temperature when bulk temperature should be used in estimating ΔT_{water} , such “skin effects” will introduce error into our estimate of Q_{ocean} . However, Fig. 9 shows that error in ΔT_{water} of 0.1–1.5°C should result in negligible error in the estimation of Q_{ocean} . Residence times show that heat at the distal end of the warm water plumes was generated 4–7 h previously. Water at the distal end of the plume is $\sim 1260 \text{ m}$ off-shore of the heat source, given a current velocity of 0.05 m s^{-1} ; this water must have been heated at the source $2.52 \times 10^4 \text{ s}$ previously. Because we are only interested in heat lost by currently moving flows, we use those pixels within which water was heated within $0.2 \pm 0.1 \text{ h}$. By using the pixels with the maximum ΔT_{water} at each of the ocean-entry points, this allows the thermal flux released within the last 0.2 ± 0.1 hours to be estimated. This gives Q_{ocean} of $2.7 \times 10^8 \text{ W}$, where Q_{vap} accounts for 12% of this total (Fig. 10).

Effusion rates and thermal flux

Effusion rates estimated using VLF electromagnetic induction (Kauahikaua et al. 1996) give results of 1.36 and $0.89 \text{ m}^3 \text{ s}^{-1}$ on 23 July and 11 October 1991, respectively, both estimates having errors of $\sim 10\%$ (J. Kauahikaua, pers. commun.). Using the Q_{tot} for these two dates obtained using our thermal model with the input parameters derived as described (Table 4), we obtain similar rates of 1.76 ± 0.57 and $0.78 \pm 0.27 \text{ m}^3 \text{ s}^{-1}$ on 23 July and 11 October. On 23 July we estimate that 36% of the lava was reaching the coast, flowing into the ocean at a rate of $0.65 \pm 0.20 \text{ m}^3 \text{ s}^{-1}$. Considering the contribution of each thermal flux to the total flux from the active flows at Kilauea on 23 July and 11 October 1991, we find that along tubed portions of the flow heat loss due to convection, conduction, rain, and radiation dominate (Fig. 10). Thermal loss from skylights will be significant only if the skylights are numerous enough. For surface flows, heat loss due to radiation, forced convection, and conduction are significant, and for submarine flows heat lost to the water and vapor plume must be considered. All other fluxes are negligible (Fig. 10). Considering just these most significant thermal fluxes in the thermal/effusion rate model would make little difference to the calculated effusion rate. Once all parameters have been set, our software and calculations then take approximately 1 h to complete.

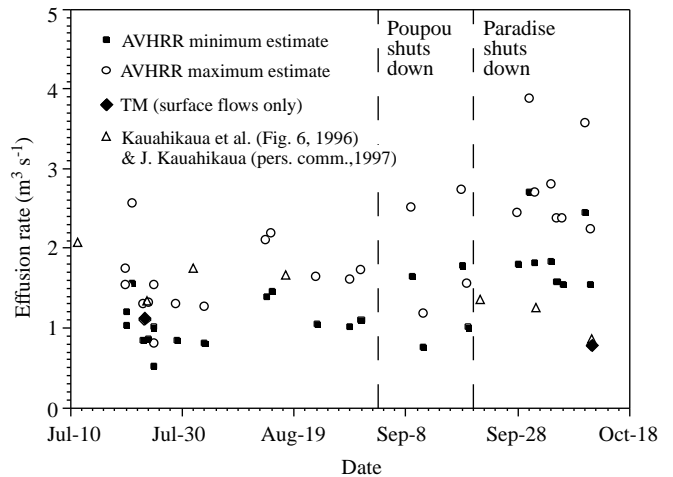


Fig. 14 Effusion rates for surface flows only calculated by applying the method of Harris et al. (1997b) to cloud-free AVHRR images of the Pu’u ’O’o–Kupaianaha flow field acquired between July and October 1991. This method gives a range of effusion rate estimates, the upper and lower limits of which are given by *open circles* and *black squares*, respectively. Effusion rates calculated using TM data (*black diamonds*) and taken from Kauahikaua et al. (1996, Fig. 6) and J. Kauahikaua (pers. commun.; *open triangles*) for surface flows are given for comparison

To determine whether these effusion rates were typical between July and October 1991, we applied the approach of Harris et al. (1997b) to calculate effusion rates from 26 cloud-free AVHRR images of this flow field acquired during this time. The spatial resolution of these images is too poor to resolve the ocean-entry anomaly; hence, our thermal flux and effusion rate estimates are for subaerial flows only (Fig. 14). The AVHRR-derived effusion rate time series was in close agreement with those effusion rates for subaerial flows obtained by us and by Kauahikaua et al. (1996). Prior to the shut down of the Paradise ocean entry, the AVHRR-based estimates are in agreement with those obtained from TM data and ground-based techniques (Fig. 14). Although after this shut-down the AVHRR estimates are 0.2 – $1.0 \text{ m}^3 \text{ s}^{-1}$ higher than other estimates, we feel that this is a reasonable error given the spatial resolution of the AVHRR data and the slight (up to $\sim 1 \text{ m}^3 \text{ s}^{-1}$) temporal variations in effusion rates over a few hours or days.

If the anomalously high AVHRR-derived effusion rates of 30 September and 10 October are ignored, then the time series show that effusion rates for land-based flows over this period were fairly stable, the decline between the two TM-derived rates being just 1.1 – $0.9 \text{ m}^3 \text{ s}^{-1}$ (Fig. 14). Since, between July and October 1991, total effusion rates at the Pu’u ’O’o–Kupaianaha flow field declined (from ~ 1.4 to $\sim 0.9 \text{ m}^3 \text{ s}^{-1}$), stable effusion rates for surface flows must have been achieved by shut-down of the ocean entries. We suggest that the decline in effusion rates caused the entries to shut down. However, the stable supply to subaerial flows (Fig. 14) enabled similar, or even slightly in-

Table 4 Input parameters necessary to calculate lava flow thermal flux and effusion rate using our model

Constants		Variables (set using field data)	
Parameter	Value	Parameter	Derivation
ρ_{lava}	$\sim 2600 \text{ kg/m}^3$	ΔT_{stop} ($= T_{\text{erupt}} - T_{\text{stop}}$)	Set using typical T_{erupt} for the lava composition erupted (i.e., basalt = 1000–1200 °C, andesite = 950–1200 °C, dacite = 800–1100 °C, rhyolite = 700–900 °C) with T_{stop} of ~ 800 °C
$c_{p\text{lava}}$	$\sim 1225 \text{ J/kg}\cdot\text{K}$	$\Delta \phi$	Set using petrological data from lava samples typical of the those erupted at the volcano analyzed
C_L	$3 \times 10^5 \text{ J/kg}$	$D_{\text{tube}}, H_{\text{tube}}, r_{\text{tube}}$	Set using field observations of tube systems
$\alpha_{\text{air}}, \mu_{\text{air}}, \kappa_{\text{air}}$	Set from published tables	A_{100}	Set using local rainfall data
$\beta_{\text{air}}, c_{p\text{air}}$	Set from published tables	$\partial R/\partial t$	Set from field measurements,
g	9.8 m/s^2	T_{sky}	where $T_{\text{tube}} (= T_{\text{erupt}})$ to 900 °C is a reasonable range for T_{sky}
K_{lava}	10^{-11} m^2	ΔT_{sky} ($= T_{\text{sky}} - T_{\text{air}}$)	T_{air} is set using typical local air temperatures from meteorological records
κ_{lava}	$\sim 3 \text{ W/mK}$	U	Set using local wind-speed data
β_{lava}	${}^n \kappa_{\text{lava}} = /(\rho_{\text{lava}} c_{p\text{lava}})$	ΔT_{base} ($= T_{\text{cb}} - T_{\text{base}}$)	Set using T_{cb} , the temperature at the base of the core (approximated by $T_{\text{erupt}} - 100$ °C), and T_{base} , the temperature at the contact between the flow and the underlying rock (~ 800 °C for pahoehoe)
$\rho_{\text{H}_2\text{O}}$	958 kg/m^3	$F_{\text{gas}}, F_{\text{H}_2\text{O}}$	Set using estimated gas flux from the flow obtained from field data
$L_{\text{H}_2\text{O}+}$	2.8 MJ/kg	ΔT_{gas} ($= T_{\text{gas}} - T_{\text{air}}$)	Where T_{gas} will approximate T_{erupt}
$L_{\text{H}_2\text{O}}$	2.26 MJ/kg		
σ	$5.67 \pm 10^{-8} \text{ W/m}^2\text{K}^4$		
T_{bound}	$= 42.605 + 0.6103T_c$		
C_{H}	$= (U^*/U)^2$, where (U^*/U) is ~ 0.06		
$c_{p\text{gas}}$	1600 J/Kg K		
ρ_{water}	1020 kg/m^3		
$c_{p\text{water}}$	4005 J/kg K		
	0.9 (for basaltic pahoehoe)		
Variables (set using TM data)		Variables (set using TM and field data)	
Parameter	Derivation	Parameter	Derivation
L_{tube}	Measured (see Table 2)	ΔT_{tube} ($= T_{\text{tube}} - T_{\text{surf}}$)	Where T_{tube} is taken from field data and T_{surf} is obtained from TM
A_{sky}	Calculated (see Table 2)	ΔT_{f} ($= T_c - T_{\text{air}}$)	Where T_{air} is assumed from meteorological data and T_c is estimated using TM data
A_{pixel}	See Table 1	V_{water} ($= H_{\text{plume}} \times \text{Area}$)	Where H_{plume} is the height of the warm water plume and is assumed from field data and Area is the area of the plume which can be measured using TM data
f_c	Calculated	R ($= L_{\text{water}}/C_v$)	Where L_{water} is measured using TM data and C_v is assumed from field data
f_{hi}	Calculated	V_{vap} ($= \text{vap} \times V_{\text{water}}$)	Where vap is the fraction of V_{water} which is vaporized and is assumed from field measurements
T_c	Calculated		
T_{hi}	Assumed: 900 ± 100 °C		
h_{base}	Estimated as a function of T_c		
A_{flow}	Measured (see Table 2)		
ΔT_{water} ($= T_{\text{plume}} - T_{\text{ocean}}$)	Where T_{plume} and T_{ocean} are estimated using TM		
T_c	$= [f_c T_c^4 + f_{\text{hi}} T_{\text{hi}}^4]^{0.25}$		

^v parameter should be corrected for vesicularity, where the vesicularity typical of the flows erupted at the volcano being analyzed should be used

creased, areal coverage by subaerial flows between July and October 1991 (Table 2), despite an overall reduction in effusion rates.

Conclusion

Using our thermal model we obtain effusion rates of 1.76 ± 0.57 and $0.78 \pm 0.27 \text{ m}^3 \text{ s}^{-1}$ for lava flows at Kilauea on 23 July and 11 October 1991, respectively.

These rates compare with field measurements of 1.36 and $0.89 \text{ m}^3 \text{ s}^{-1}$ for the same dates (Kauahikaua et al. 1996).

We used input parameters from TM and field data for the active flows at Kilauea, however we assume that the models to calculate total thermal flux from an active lava flow and effusion rates should be universally applicable. We used the Kilauea example to show how input parameters can be set (Table 4) and to test the accuracy of the model through comparison with availa-

ble field measurements of effusion rates. Close agreement with field-based measurements show that reliable effusion rates can be obtained using our approach. The constants (Table 4) should be universally applicable to any basaltic eruption. Since TM data are potentially available for any volcano once every 16 days, those variables set using TM data (Table 4) can be calculated if a cloud-free TM image is available. Other parameters need to be estimated from other means, e.g., ground or air-borne observations (Table 4). However, we believe that the synoptic and regular coverage given by the satellite perspective provides the most efficient way to measure flow-wide thermal and dimension parameters. We note that synergy is required between field data and remote sensing for the quantification of input parameters; our approach is not possible unless adequate field data are available.

Our models can be easily modified to accept data from a constellation of new instruments under development in NASA's Mission to Planet Earth program. This will offer much greater access to both high spatial and high temporal resolution data sets. In terms of high spatial resolution data, Landsat 7 (1998 launch) and the Advanced Spaceborne Thermal Emission and Reflection Radiometer (1998 launch) will continue to provide data in similar spectral regions and bandwidths to Landsat 5. The Hyperspectral Imager (1997 launch) and the Advanced Land Imager (1999? launch) are hyperspectral instruments that will measure radiance in hundreds of channels across the 0.4- to 2.5- μm region of the spectrum. The increased spectral resolution of those instruments will translate into much more detailed estimates of thermal loss from individual pixels and, hence, better estimates of effusion rates.

The synergetic use of data sets from different sensors with differing spatial and temporal resolutions, such as the TM and AVHRR, provide an integrated data set that is both spatially and temporally detailed. Such a data set allows flow-field evolution to be monitored and various flow-field parameters to be measured. The synoptic coverage of the data, allowing flow-wide analysis, makes the data a potentially useful addition to current monitoring techniques, capable of contributing to spatial and temporal analyses of flow-field evolution. We look forward to the availability of MODIS in 1998, which will offer complete global coverage every 2 days in 36 spectral channels at 250-, 500-, or 1000-m spatial resolutions, with more frequent coverage near the poles.

Appendix A

The pixel-integrated temperature of a mixed TM band-6 pixel containing land at temperature T_{land} and water at temperature T_{water} ($=T_{\text{plume}}$ or T_{ocean}) can be described by:

$$L(\lambda_6 T_m) = f_{\text{land}} L(\lambda_6 T_{\text{land}}) + (1 - f_{\text{land}}) L(\lambda_6 T_{\text{water}}),$$

in which $L(\lambda T)$ is the Planck function radiance for a blackbody at wavelength λ and temperature T , λ_6 is the TM band-6 central wavelength, T_m is the pixel integrated temperature of the mixed pixel, and f_{land} is the fraction of the pixel covered by land. Rearranging allows T_{water} to be calculated from

$$L(\lambda_6 T_{\text{water}}) = \frac{L(\lambda_6 T_m) - f_{\text{land}} L(\lambda_6 T_{\text{land}})}{[1 - f_{\text{land}}]}.$$

We set T_{land} by using the mean temperature of the nearest band-6 pixels which contain purely land and f_{land} by counting the number of 900- m^2 TM band-1 to band-5 pixels within the 14400 m^2 band-6 pixel that are covered by land (n_{L900}), then

$$f_{\text{land}} = n_{\text{L900}} \times A_{900} / A_6.$$

A_{900} and A_6 are the areas of band-1 to band-5 pixels, and band-6 pixels, respectively (i.e., 900 and 14400 m^2).

Acknowledgements We are grateful to P. Flament (SOEST, University of Hawaii) for supplying the AVHRR images used in this study, H. Garbeil (HIGP, University of Hawaii) for unpacking the images and setting up the processing software, and J. Kauhikaua (HVO) for providing valuable unpublished field observations. Field measurements made during October 1995 were funded by ODA (U.K.) grant R5989. We thank D. Rothery and M. Wooster (both from Open University) for help and valuable discussions in the field. We are grateful to J. Salisbury (Johns Hopkins University) for providing pahoehoe spectra and to G. Wadge (Reading University) and S. Drury (Open University) for valuable input and initial suggestions. Thanks also to L. Glaze, D. Pieri, and D. Rothery for their helpful reviews. L. P. K.'s work was made possible by the volunteer program of the U.S. Geological Survey and the assistance and hospitality of the Hawaiian Volcano Observatory. Funding for J. A. R. was provided by Office of Naval Research (grant no. N00014-96-10352 to J. Resing via Y. H. Li). Funding for A. J. L. H. and L. P. F. was provided by NASA grant NAG 5-3451 for Landsat Science Team. This is SOEST contribution no. 4573 and HIGP contribution no. 972.

References

- Andres RJ, Rose WI (1995) Description of thermal anomalies on two active Guatemalan volcanoes using Landsat Thematic Mapper imagery. *Am Soc Photogram Eng* 61:775-782
- Arya SPS (1988) Introduction to micrometeorology. Academic Press, Orlando, pp 1-307
- Barberi F, Carapezza ML, Valenza M, Villari L (1993) The control of lava flow during the 1991-1992 eruption of Mt. Etna. *J Volcanol Geotherm Res* 56:1-34
- Bhattacharya A, Reddy CSS, Srivastav SK (1993) Remote sensing for active volcano monitoring in Barren Island, India. *Photogram Eng Remote Sensing* 59:1293-1297
- Brandeis G, Jaupart C, Allegre CJ (1984) Nucleation, crystal growth and the thermal regime of cooling magmas. *J Geophys Res* 89:10161-10177
- Calvari S, Coltelli M, Neri M, Pompilio M, Scribano V (1994) The 1991-1993 Etna eruption: chronology and lava flow-field evolution. *Acta Vulcanol* 4:1-14
- Cashman KV, Mangan MT, Newman S (1994) Surface degassing and modifications to vesicle size distributions in active basalt flows. *J Volcanol Geotherm Res* 61:45-68

- Crisp J, Baloga S (1990) A model for lava flows with two thermal components. *J Geophys Res* 95:1255–1270
- Crisp J, Baloga S (1994) Influence of crystallization and entrainment of cooler material on the emplacement of basaltic aa lava flows. *J Geophys Res* 99:11819–11831
- Danes ZF (1972) Dynamics of lava flows. *J Geophys Res* 77:1430–1432
- Dozier J (1981) A method for satellite identification of surface temperature fields of subpixel resolution. *Remote Sensing Environ* 11:221–229
- Flynn LP, Mouginiis-Mark PJ (1992) Cooling rate of an active Hawaiian lava flow from nighttime spectroradiometer measurements. *Geophys Res Lett* 19:1783–1786
- Flynn LP, Mouginiis-Mark PJ (1993) Temperature of an active lava channel from spectral measurements, Kilauea Volcano, Hawaii. *Bull Volcanol* 56:297–301
- Flynn LP, Mouginiis-Mark PJ, Horton KA (1994) Distribution of thermal areas on an active lava flow field: Landsat observations of Kilauea, Hawaii, July 1991. *Bull Volcanol* 56:284–296
- Frazzetta G, Romano R (1984) The 1983 Etna eruption: event chronology and morphological evolution of the lava flow. *Bull Volcanol* 47:1079–1096
- Glaze L, Francis PW, Rothery DA (1989) Measuring thermal budgets of active volcanoes by satellite remote sensing. *Nature* 338:144–146
- Greeley R, Iversen JD (1987) Measurements of wind friction speeds over lava surfaces and assessment of sediment transport. *Geophys Res Lett* 14:925–928
- Gupta RK, Badarinath KVS (1993) Volcano monitoring using remote sensing data. *Int J Remote Sensing* 14:2907–2918
- GVN (1990a) Kilauea. Smithsonian Institution Bull. *Global Volcanol Net* 15 (8): 7–9
- GVN (1990b) Kilauea. Smithsonian Institution Bull. *Global Volcanol Net* 15 (10): 10–11
- GVN (1991a) Kilauea. Smithsonian Institution Bull. *Global Volcanol Net* 16 (5): 20
- GVN (1991b) Kilauea. Smithsonian Institution Bull. *Global Volcanol Net* 16 (7): 9–10
- GVN (1991c) Kilauea. Smithsonian Institution Bull. *Global Volcanol Net* 16 (8): 17–18
- GVN (1991d) Kilauea. Smithsonian Institution Bull. *Global Volcanol Net* 16 (9): 5–6
- GVN (1991e) Kilauea. Smithsonian Institution Bull. *Global Volcanol Net* 16 (10): 8–9
- Harris AJL, Stevenson DS (1997) Thermal observations of degassing open conduits and fumaroles at Stromboli and Vulcano using remotely sensed data. *J Volcanol Geotherm Res* 76:175–198
- Harris AJL, Vaughan RA, Rothery DA (1995) Volcano detection and monitoring using AVHRR data: the Krafla eruption, 1984. *Int J Remote Sensing* 16:1001–1020
- Harris AJL, Butterworth AL, Carlton RW, Downey I, Miller P, Navarro P, Rothery DA (1997a) Low-cost volcano surveillance from space: case studies from Etna, Krafla, Cerro Negro, Fogo, Lascar and Erebus. *Bull Volcanol* 59:49–64
- Harris AJL, Blake S, Rothery DA, Stevens, NF (1997b) A chronology of the 1991 to 1993 Etna eruption using AVHRR data: implications for real time thermal volcano monitoring. *J Geophys Res* 102:7985–8003
- Head JW III, Wilson L (1986) Volcanic processes and landforms on Venus: theory, predictions, and observations. *J Geophys Res* 91:9407–9446
- Heliker C, Wright TL (1991) The Pu'u 'O'o-Kupaianaha eruption of Kilauea. *EOS* 72:521–530
- Helz R, Thornber C (1987) Geothermometry of Kilauea Iki lava lake, Hawaii. *Bull Volcanol* 49:651–668
- Helz RT, Heliker C, Mangan M, Hon K, Neal CA, Simmons L (1991) Thermal history of the current Kilauean East Rift eruption. *EOS Trans AGU* 72:557–558
- Holman JP (1992) Heat transfer. McGraw-Hill, London, pp 1–713
- Hon K, Kauahikaua J, Mackay K (1993) Inflation and cooling data from pahoehoe sheet flows on Kilauea Volcano. US Geol Surv Open-File Rep 93–342A (paper copy) or OF93-342B (3.5" IBM-compatible diskette): 1–16
- Hon K, Kauahikaua J, Denlinger R, Mackay K (1994) Emplacement and inflation of pahoehoe sheet flows: observations and measurements of active lava flows on Kilauea Volcano, Hawaii. *Geol Soc Am Bull* 106:351–370
- Huppert HE, Sparks RSJ (1988) The generation of granitic magmas by intrusion of basalt into continental crust. *J Petrol* 29:599–624
- Jaeger JC (1961) The cooling of irregularly shaped igneous bodies. *Am J Sci* 259:721–734
- Kauahikaua J, Mangan M, Heliker C, Mattox T (1996) A quantitative look at the demise of a basaltic vent: the death of Kupaianaha, Kilauea Volcano, Hawaii. *Bull Volcanol* 57:641–648
- Kays WM, Crawford ME (1980) Convective heat and mass transfer. McGraw-Hill, New York, 1–420
- Keszthelyi L (1995a) A preliminary thermal budget for lava tubes on the Earth and planets. *J Geophys Res* 100:20411–20420
- Keszthelyi L (1995b) Measurements of the cooling at the base of pahoehoe flows. *Geophys Res Lett* 22:2195–2198
- Keszthelyi L, Denlinger R (1996) The initial cooling of pahoehoe flow lobes. *Bull Volcanol* 58:5–18
- Kirkpatrick RJ (1976) Towards a kinetic model for the crystallization of magma bodies. *J Geophys Res* 81:2565–2571
- Lipman PW, Banks NG (1987) AA flow dynamics, Mauna Loa 1984. US Geol Surv Prof Pap 1350: pp. 1527–1567
- Malin MC (1980) Lengths of Hawaiian flows. *Geology* 8:306–308
- Mangan MT, Cashman KV, Newman S (1993) Vesiculation of basaltic magma during eruption. *Geology* 21:157–160
- Mangan MT, Heliker CC, Mattox TN, Kauahikaua JP, Helz RT (1995) Episode 49 of the Pu'u 'O'o-Kupaianaha eruption of Kilauea Volcano: breakdown of a steady-state eruptive era. *Bull Volcanol* 57:127–135
- Mattox TN, Heliker C, Kauahikaua J, Hon K (1993) Development of the 1990 Kalapana flow field, Kilauea Volcano, Hawaii. *Bull Volcanol* 55:407–413
- McClelland L, Simkin T, Summers M, Nielsen E, Stein TC (1989) Global volcanism 1975–1985. Prentice-Hall, Englewood Cliffs, New Jersey
- Oppenheimer C (1991) Lava flow cooling estimated from Landsat Thematic Mapper infrared data: the Lonquimay eruption (Chile, 1989). *J Geophys Res* 96:21865–21878
- Oppenheimer C (1997) Ramifications of the skin effect for crater lake heat budget analysis. *J Volcanol Geotherm Res* 75:159–165
- Oppenheimer C, Francis PW, Rothery DA, Carlton RWT, Glaze LS (1993) Infrared image analysis of volcanic thermal features: Lascar Volcano, Chile, 1984–1992. *J Geophys Res* 98:4269–4286
- Paulson CA, Simpson JJ (1981) The temperature difference across the cool skin of the ocean. *J Geophys Res* 86:11044–11054
- Pieri DC, Baloga SM (1986) Eruption rate, area and length relationships for some Hawaiian lava flows. *J Volcanol Geotherm Res* 30:29–45
- Pieri DC, Glaze LS, Abrams MJ (1990) Thermal radiance observations of an active lava flow during the June 1984 eruption of Mount Etna. *Geology* 18:1018–1022
- Peck DL (1978) Cooling and vesiculation of Alae lava lake, Hawaii. US Geol Surv Prof Pap 935-B: 1–59
- Peck DL, Wright TL, Moore JG (1966) Crystallization of the tholeiitic basalt in Alae lava lake, Hawaii. *Bull Volcanol* 29:629–655
- Peck DL, Hamilton MS, Shaw HR (1977) Numerical analysis of lava lake cooling models. Part II. Application to Alae lava lake, Hawaii. *Am J Sci* 277:415–437

- Pinkerton H, Sparks RSJ (1976) The 1975 sub-terminal lavas, Mount Etna: a case history of the formation of a compound lava field. *J Volcanol Geotherm Res* 1:167–182
- Pinkerton H, Wilson L (1994) Factors controlling the lengths of channel-fed lava flows. *Bull Volcanol* 56:108–120
- Resing JA (1997) The chemistry of lava–seawater interactions at the shoreline of Kilauea Volcano, Hawaii. PhD thesis, University of Hawaii, 258 pp
- Reynolds RW, Geist D, Kurz MD (1995) Physical volcanology and structural development of Sierra Negra Volcano, Isabela Island, Galápagos archipelago. *Geol Soc Am Bull* 107:1398–1410
- Rothery DA, Francis PW, Wood CA (1988) Volcano monitoring using short wavelength infrared data from satellites. *J Geophys Res* 93:7993–8008
- Rowland SK (1996) Slopes, lava flow volumes, and vent distributions on Volcan Fernandina, Galápagos Islands. *J Geophys Res* 101:27657–27672
- Rowland SK, Munro DC (1993) The 1919–1920 eruption of Mauna Iki, Kilauea: chronology, geologic mapping, and magma transport mechanisms. *Bull Volcanol* 55:190–203
- Rowland SK, Walker GPL (1990) Pahoehoe and aa in Hawaii: volumetric flow rate controls the lava structure. *Bull Volcanol* 52:615–628
- Sansone FJ, Resing JA (1995) Hydrography and geochemistry of sea surface hydrothermal plumes resulting from Hawaiian coastal volcanism. *J Geophys Res* 100:13555–13569
- Sansone FJ, Resing JA, Tribble GW, Sedwick PN, Kelly KM, Hon K (1991) Lava–seawater interactions at shallow-water submarine lava flows. *Geophys Res Lett* 18:1731–1734
- Schluessel P, Emery WJ, Grassl H, Mammen T (1990) On the bulk-skin temperature difference and its impact on satellite remote sensing of sea surface temperature. *J Geophys Res* 95:13341–13356
- Shaw HR, Hamilton MS, Peck DL (1977) Numerical analysis of lava lake cooling models. Part I. Description of the method. *Am J Sci* 277:384–414
- Wadge G (1978) Effusion rate and the shape of aa lava flow-fields on Mount Etna. *Geology* 6:503–506
- Wadge G (1981) The variation of magma discharge during basaltic eruptions. *J Volcanol Geotherm Res* 11:139–168
- Walker GPL (1973) Lengths of lava flows. *Phil Trans R Soc Lond* 274:107–118
- Wilmoth RA, Walker GPL (1993) P-type and S-type pahoehoe: a study of vesicle distribution patterns in Hawaiian lava flows. *J Volcanol Geotherm Res* 55:129–142
- Wilson L, Head JW III (1994) Mars: review and analysis of volcanic eruption theory and relationships to observed landforms. *Rev Geophys* 32:221–263
- Wolfe EW, Neal CA, Banks NG, Duggan TJ (1988) Geologic observations and chronology of events. US Geol Surv Prof Pap 1463:1–97
- Wright TL, Okamura RT (1977) Cooling and crystallization of tholeiitic basalt, 1965 Makaopuhi lava lake, Hawaii. US Geol Surv Prof Pap 1004:pp 1–78